Doctoral Dissertation

Studies on Enhanced Performance of a Stand-Alone Gas Engine Generator with a Permanent Magnet Synchronous Generator by Applying Active Rectifier and Virtual Synchronous Generator Control

Htar Su Hlaing

January, 2020

Graduate School of Engineering

Osaka University

Abstract

Gas engine generators are widely used in the field of emergency power supplies and combined heat and power applications. They can also serve as main power sources in places where utility power is not available. Moreover, compared to diesel engines, gas engines are more environment-friendly as they release low exhaust emissions. A gas engine generator consists of a mechanical part (engine) and an electrical part (generator). Different kinds of generators can be used to convert the engine's mechanical energy to the electrical energy. Among them, the permanent magnet synchronous generator (PMSG) provides the advantages of no excitation current, small size, less weight and high efficiency.

Despite the effectiveness of gas engine generators, they cannot fully provide their advantages to the system. The reason is the engine's delayed response to the sudden load changes. The gas engine has a time constant of a few seconds to reach the demanded torque due to the fuel injection function. Consequently, the speed deviation is large during load transitions. If the speed variation is larger than the permitted limits, the operation will be shut down. Therefore, for the current users of gas engines, the load step capability is restricted in order to maintain the engine speed variation within the allowable limits. For this reason, the transient behavior of gas engine becomes a major challenge in using gas engines.

To improve the transient performance of gas engine, this dissertation proposes a virtual synchronous generator (VSG) control method to the stand-alone gas engine generator. To reduce the engine speed deviation, an electric double layer capacitor (EDLC) based energy storage system (ESS) is added at the dc-link of the system. A PMSG control approach is developed to control both the dc-link voltage and the stator voltage by applying the insulated gate bipolar transistors (IGBTs)-based active rectifier, instead of a diode rectifier. Furthermore, the control characteristics of different control methods of PMSG are also evaluated.

The structure of this dissertation is organized as follows:

In chapter 1, the research background, an overview of previous research works, the problem issues of gas engine generator and the objectives of this research are described.

In chapter 2, the VSG control method combined with an ESS is proposed for the stand-alone operation of gas engine generator. The benefit of VSG control method for the proposed system is evaluated and the outcomes are compared with the results of the same system using a constant-voltage constant-frequency (CVCF) control method. An energy variables based feedback control is proposed for the control of energy storage

system. The required amount of energy storage capacity is calculated based on the demanded load power. A simulation study and an experimental test are carried out to verify the usefulness of the proposed control scheme.

In chapter 3, an active rectifier is used for the ac-dc power conversion in order to improve the stator current waveform of the engine generator. This system provides the full controllability and improves the efficiency and reliability of the system. For the control of PMSG side converter, the constant stator voltage (CSV) control is proposed. The VSG control method is used for the control of load side converter. The transient performance of the proposed system is compared with that of the system using a diode rectifier in simulation study.

In chapter 4, some different control schemes of PMSG are studied. The two control concepts of zero d-axis current (ZDC) control method and unity power factor (UPF) control method are explained. The system responses of the mentioned control methods are evaluated by computer simulation.

In chapter 5, thesis outcomes are summarized and the conclusion of this dissertation is presented.

Table of Contents

Chapter 1
Introduction

Recently, the distributed generation (DG) systems have been developed for the issues of energy crisis and environmental reasons [1]. These systems consist of renewable and non-renewable energy resources. Solar energy and wind energy are the most popular renewable resources in the DG system. However, these energy resources are weather dependent and cannot guarantee a stable power supply at all time. The non-renewable energy resources such as reciprocating internal combustion engines can provide a stable power supply. In general, the power generation from reciprocating engines can be found in the regions where the main power supply cannot be accessed. As they are mobile power generation units, they are also popular for the applications of emergency power supplies and combined heat and power (CHP) systems.

Basically, there are two types of internal combustion engines: compression ignition typed diesel engines and spark ignition typed gas engines. For many years, the diesel engines are commonly used for power generation in the world wide. At the present time, the applications of diesel engines become restricted in most countries because of CO_2 emission concerns. From environmental issues point of view, the gas engines release low CO_2 emissions compared to the diesel engines [2-3]. In addition, the large amount of natural gas is available from shale deposits in several countries of the world which makes the natural gas to be low-cost [4]. For their low CO_2 emission and appropriate fuel price, the gas engines are more likely to be employed in the future power generation systems. Thus, in this thesis, the performance of gas engine that is operated in stand-alone system is investigated.

1.1 Background

The topologies of a microgrid with gas engine generation are presented in [5]. In [5], four topologies of a microgrid structure are presented and some qualitative comparisons of these structures are described. The results of comparisons show that the adventitious topologies are to connect the gas engine via a power electronics unit to the grid or to the load rather than a direct connection. In practice, two schemes of power electronics units are commonly employed in the gas engine generators [6]. The first scheme is a diode rectifier followed by an inverter through a dc-link as shown in Fig. 1.1(a). In the second scheme, the insulated gate bipolar transistors (IGBTs) based rectifier which is known as an active rectifier is followed by an inverter via a dc-link as shown in Fig. 1.1(b).

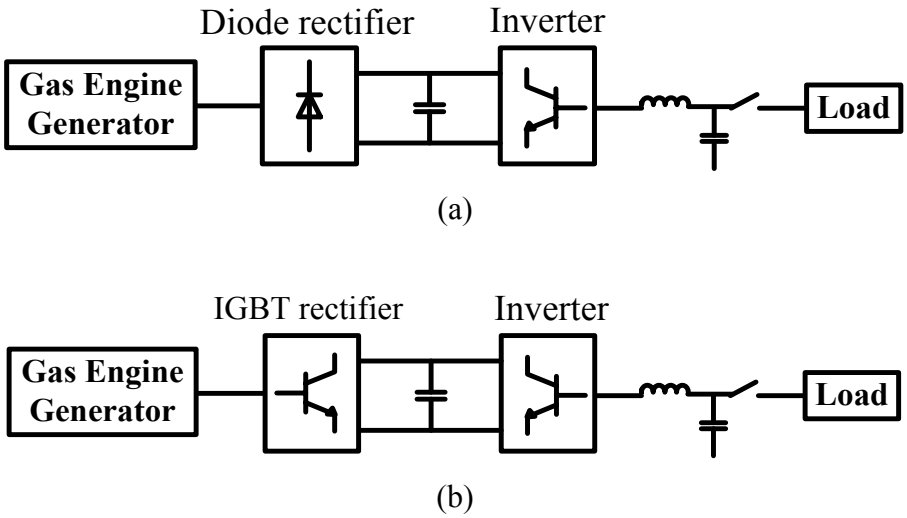

Figure 1.1 (a) Configuration of gas engine generator with diode rectifier and inverter, (b) Configuration of gas engine with IGBT rectifier and inverter

In gas engine generator with an active rectifier system, the generator side converter control mainly depends on the type of generator connected to the engine. The operation of reciprocating engines is initiated with a conventional synchronous generator (SG). Following the increasingly use of the permanent magnet synchronous generator (PMSG) and doubly-fed induction generator (DFIG) in the wind power applications, these types of generators are becoming to spread in the reciprocating engine generator systems. The applications of DFIG for stand-alone gas engine system can be found in [7-8]. The applications of PMSG for the diesel engine generator system are explained in [9-10]. Compared to other types of generators, the PMSG has been increasingly used in wind power systems owing to its higher efficiency, no excitation losses, smaller size, and less weight.

The load side or the grid side converter control framework depends on whether the gas engine generator is in the grid-connected operation or in the stand-alone operation. In the grid-connected system, the distributed power source follows the voltage and the frequency determined by the SG of the system. Generally, the inverter of the distributed power source is controlled by a simple current control method. By the current control method, the inverter output power can be directly controlled by using the grid voltage. On the other hand, the output voltage and frequency of inverter rely on the grid voltage and frequency. Therefore, this method cannot be applied for the stand-alone operation. Furthermore, the system becomes unstable because of decreasing inertia when the number of distributed power sources increases in the system.

For the stand-alone operation, the voltage and frequency references of the inverter are determined by itself. Thus, the output power of the inverter is normally controlled by the constant-voltage constant-frequency (CVCF) control method. In this control

method, the inverter output voltage and frequency are controlled to follow the base voltage and frequency of the inverter. By this control method, the synchronization with the grid is not possible and the interconnection with the grid cannot be able without stopping the generator operation.

Recently, the concept of virtual synchronous generator (VSG) control method which can control the inverter to behave like an SG has been developed. In this control method, the swing equation of a typical SG is realized in the inverter control scheme, and the energy storage connected to the inverter imitates the kinetic energy of rotating mass. Usually, the energy storage is the dc link capacitor. In some cases where the large amount of energy is required, a battery or a supercapacitor can be added to the dc link capacitor. By this way, like an SG, the VSG controlled inverter can not only function in stand-alone mode but also can be synchronized with the grid, and can provide inertia for the utility stabilization [11]-[13].

1.2 Review on the previous research works

In most previous research works, the VSG control method is employed either without considering the features of energy resources [14]-[16], or only focuses on the grid-connected systems [21]-[26]. Only some research works are focused on using the VSG method for the stand-alone system considering the characteristics of the energy resources [17]-[18]. The VSG control method for parallel diesel engines is found in [19]. In [20], the VSG control is proposed for the control of grid side converter for a full converter wind turbine (FCWT). The proposed VSG control method allows the system to operate under both grid-connected and stand-alone conditions. In [21], the problems of matching photovoltaic (PV) output and load as well as dc voltage collapse are solved by the VSG control in a stand-alone PV system.

The performance of PMSG in wind power systems is also investigated by applying various control approaches to the generator side converter [22]-[28]. A variable-speed PMSG system with a diode rectifier that is connected to a dc chopper is studied in [22]. Despite a simple and low-cost solution, this system outputs high harmonic distortion current which affects the generator efficiency. In [23], the dynamic performance of a grid-connected PMSG wind energy system is investigated by using a fully controllable frequency converter. The generator side converter is controlled to reduce the stator flux and minimize core losses by imposing the reactive current on d-axis component.

In [24-26], the zero d-axis control (ZDC) approach is adopted for the control of PMSG to minimize power losses and maximize available torque. In [27], the unity power factor (UPF) control approach is adopted for the PMSG side converter. This control approach can also help the system to minimize power losses and maximize

available torque. In [28], a constant stator voltage (CSV) control strategy is proposed for the control of PMSG side converter. In [29], the PMSG controlled by the UPF method is applied to the internal combustion engine generator system.

1.3 Problem statement

In power generation, as the gas engine drives the generator to generate the alternating current (AC) power, the gas engine generator system is a combination of a mechanical system (the fuel injection function and engine) and an electrical system (generator).

An important issue in using gas engine generator deals with the engine's mechanical system. The engine's mechanical system has a delayed response to the sudden load changes. The reason is that the engine has a time constant of a few seconds to reach the demanded torque due to the fuel injection function. Consequently, a large engine speed deviation occurs during load transitions, especially in the stand-alone operation. If the speed variation is larger than the permitted limits, the operation will be shut down. For this reason, the transient behavior of gas engine is a major challenge in using this type of engine.

The general transient response requirements of gas engines are presented in [30]. The step load responses of two types of gas engines and one diesel engine are also compared in [30]. The results show that the gas engine has longer recovery time and larger frequency excursion than the diesel engine. In [31], the start-up time reduction of a gas engine is analyzed with the aim of improving transient response. As an option of providing the demanded power without delay, the use of energy storage system (ESS) in combination with engine is suggested. This option is a solution to the transient issues that deal with the slow response of engine's thermal and mechanical system by the help of electrical system.

In electrical system, as mentioned in Section 1.1, for the ac-dc-ac power conversion, two schemes of power electronics unit are commonly used in the gas engine generators. In the gas engine generator system with a diode rectifier followed by an inverter via a dc-link, only the load side or the grid side converter can be controlled as the generator side converter is uncontrollable. Moreover, the diode rectifier can cause high harmonic distortion in the generator currents. This leads to torque oscillations and overheating in the generator windings. As a consequence, the generator efficiency is affected. In the gas engine system with the Insulated Gate Bipolar Transistors (IGBTs)-based rectifier, both the generator side converter and the load side or the grid side converter can be controlled to achieve a desirable performance and a high reliability of the system. As a significant result, the harmonic distortions in the generator currents can be reduced by controlling the generator side converter in a proper way [32].

In order to provide an efficient generation to the users, the applied control strategies for both generator and load side converters are also important issues in using the gas engine generator.

1.4 Research objectives

As the gas engine with a PMSG is a developing system, the control strategies of this system need to be investigated for the performance improvement of the system, because the transient response of gas engine is still a major challenge in power generation. Therefore, this thesis is mainly focused on the following objectives and achievements:

(1) The recent promising VSG control concept is applied for the control of load side converter in the stand-alone gas engine with a PMSG. Furthermore, an external ESS is added to the dc-link of the proposed system. Therefore, a temporary energy supply is provided during transient periods and the speed variations can be reduced. Thus, this system covers the slow response of engine's mechanical dynamics by supporting energy from the electrical side. Moreover, the smooth power transitions during load transients are expected owing to the virtual inertia of VSG.

(2) Instead of using a diode rectifier, an active rectifier is applied to the PMSG side ac-dc power conversion. As the VSG control method is used in the load side converter, the dc-link voltage control is performed by the generator side converter. The generator stator voltage is also controlled to follow its rated voltage by using the constant stator voltage (CSV) control for the generator side converter. As a result, the system is fully controllable and the efficient generation can be provided to the customers.

(3) In addition to the CSV control method, the zero d-axis current (ZDC) control and the unity power factor (UPF) control methodologies can also be applied to the generator side converter. Therefore, the control characteristics of different control methods of PMSG are studied and evaluated for the proposed gas engine system.

1.5 Summary

In this chapter, the role of gas engines in the DG systems was briefly introduced. The background of this thesis was presented. The previous main research works related to this thesis were reviewed. The problem statement was given. The objectives and achievements of this thesis were described. Finally, the advantages and disadvantages of the conventional control scheme and proposed control schemes for generator and load side converters as well as in view point of engine speed deviation and inertia support are summarized in Table 1.1.

Table 1.1. Advantages and disadvantages of conventional control scheme and proposed control schemes

	Control schemes	Generator side control	Load side control	Engine speed deviation	Inertial support
Conventional	Diode rectifier + CVCF-inverter	×	○	×	×
Proposed	Diode rectifier + VSG- inverter	×	○	×	○
	Diode rectifier + VSG-inverter + ESS	×	○	○	○
	Active rectifier + VSG-inverter	○	○	×	○

References

[1] R. H. Lasseter, P. Paigi, "Microgrid: A conceptual solution," in *Proc. 35th Annul IEEE Power Electron. Specialists Conf.*, Aachen, Germany, 2004, pp. 4285-4290

[2] C. A. Hernandez-Aramburo, T. C. Green, and N. Mugniot, "Fuel consumption minimization of a microgrid," *IEEE Trans. Ind. Appl.*, vol. 41, no. 3, pp. 673-681, May/June 2005.

[3] L. Goldstein, B. Hedman, D. Knowles, S. I. Freedman, R. Woods and T. Schweizer, "Gas-fired distributed energy resource technology characterizations," *National Renewable Energy Laboratory*, http://www.osti.gov/bridge

[4] L. D. Brathwaite, "Shale-deposited natural gas: A review of potential," *California Energy Commiss.*, Sacramento, CA, USA, Feb. 2010. [Online]. Available:

http://www.energy.ca.gov/2009publications/CEC-200-2009-005/CEC-200-2009-005-SF.PDF

[5] M. Kwak and S. Sul, "Control of utility connected gas engine generation system," in *Proc. 37th Power Electronics Specialist Conf.*, Jeju (Korea), 18-22 June 2006.

[6] L. M. Tolbert1, W. A. Peterson, M. B. Scudiere, C. P. White, T. J. Theiss, J. B. Andriulli, C. W. Ayers, G. Farquharson, G. W. Ott, Larry E. Seiber, "Electronic power conversion system for an advanced mobile generator Set," in *Conf. Rec. IEEE, 36th IAS Annu. Meet.*, Chicago, IL, USA, vol. 3, Sep. 30 – Oct. 4, 2001, pp. 1763-1768.

[7] T. Daido, Y. Miura, T. Ise and Y. Sato, "Characteristics on stand-alone operation of a doubly-fed induction generator applied to adjustable speed gas engine cogeneration system," *Journal of Power Electronics*, vol. 13, no. 5, pp. 841-853, Sep. 2013.

[8] A. B. Ataji, Y. Miura, T. Ise, and H. Tanaka, "Machine parameter independent control of a grid-connected variable speed doubly-fed induction generator for gas engine generation systems," in *Proc. 2013 IEEE ECCE Asia Downunder Conf.*, Melbourne, Australia, 3-6 June 2013.

[9] M. J. Ryan and R. D. Lorenz, "A power-mapping variable-speed control technique for a constant-frequency conversion system powered by a IC engine and PM generator," *in Conf. Rec. IEEE IAS Annu. Meeting*, Rome, Italy, 2000, pp. 2376–2382.

[10] J. Leuchter, P. Bauer, V. Rerucha and V. Hajek, "Dynamic behavior modeling and verification of advanced electrical-generator set concept", *IEEE Trans. Ind. Electron.*, vol. 56, no. 1, pp. 266–279, January 2009.

[11] J. Driesen and K. Visscher, "Virtual synchronous generators", in *Proc. IEEE Power Energy Soc. 2008 Gen. Meet.: Convers. Del. Energy 21st Century*, Pittsburgh, PA, USA, Jul. 20–24, 2008, pp. 1-3.

[12] H.-P. Beck and R. Hesse, "Virtual synchronous machine," in *Proc. 9th Int.Conf. Elect. Power Quality Util.*, Barcelona, Spain, 2007, pp. 1–6.

[13] Q. Zhong, and G. Weiss, "Synchronverters: inverters that mimic synchronous generators," *IEEE Trans. Ind. Electron*., vol. 58, no. 4, pp. 1259–1267, April 2011.

[14] K. Sakimoto, Y. Miura, and T. Ise, "Stabilization of a power system including inverter type distributed generators by the virtual synchronous generator," *IEEJ Trans. Power and Energy*, vol. 132, no. 4, pp. 341–349, Apr. 2012 (in Japanese). Translated in Electrical Engineering in Japan, vol. 187, no. 3, pp. 7–17, May 2014 (in English).

[15] J. Liu, Y. Miura, H. Bevrani, and T. Ise, "Enhanced virtual synchronous generator control for parallel inverters in microgrids," *IEEE Trans. Smart Grid*, vol. 8, no. 5, pp. 2268–2277, Sept. 2017.

[16] N. Soni, S. Doolla and M. C. Chandorkar, "Improvement of transient resonse in microgrids using virtual inertia", *IEEE Trans. Power Delivery*, vol. 28, no. 3, pp. 1830–1838, July 2013.

[17] D. Chen, Y. Xu, and A. Q. Huang, "Integration of DC microgrids as virtual synchronous machines into the AC grid," *IEEE Trans. Ind. Electron.*, vol. 64, no. 9, pp. 7455–7466, Sept. 2017.

[18] M. Guan, W. Pan, J. Zhang, Q. Hao, J. Cheng, and X. Zheng, "Synchronous generator emulation control strategy for voltage source converter (VSC) stations," *IEEE Trans. Power Syst.*, vol. 30, no. 6, pp. 3093–3101, Nov. 2015.

[19] R. Shi, X. Zhang, L. Fang, H. Xu, C. Hu, Y. Tu and H. Ni, "Research on power compensation strategy for diesel generator system based on virtual synchronous generator", in *Proc. 2016 IEEE 8th International Power Electronics and Motion Control Conference (IPEMC-ECCE Asia)*, Hefei, P.R. China, May 2016.

[20] Y. Ma, W. Cao, L. Yang, F. Wang and L. M. Tolbert, "Virtual synchronous generator control of full converter wind turbines with short-term energy storage", *IEEE Trans. Ind. Electron.*, vol. 64, no. 11, pp. 8821–8831, November 2017.

[21] Y. Guo, L. Chen, K. Li, T. Zheng and S. Mei, "A novel control strategy for stand-alone photovoltaic system based on virtual synchronous generator", in *Proc. 2016 IEEE Power and Energy Society General Meeting (PESGM)*, Boston, MA, USA, 17-21 July 2016.

[22] M. E. Haque, M. Negnevitsky and K. M. Muttaqi, "A novel control strategy for a variable-speed wind turbine with a permanent-magnet synchronous generator", *IEEE Trans. Ind. Appl*., 46, pp. 331-339, 2010.

[23] M. Chinchilla, S. Arnaltes and J. C. Burgos, "Control of permanent-magnet generators applied to variable-speed wind energy systems connected to the grid", *IEEE Trans. Energy Convers*, 2006, 21, 130-135.

[24] G. Buticchi, E. Lorenzani, F. Immovilli and C. Bianchini, "Active rectifier with integrated system control for microwind power systems", *IEEE Trans. Sustainable Energy*. 2015. 6, 60-69.

[25] S. Li, T. A. Haskew, R. P. Swatloski and W. Gathings, "Optimal and direct-current vector control of direct-driven PMSG wind turbines", *IEEE Trans. Power Electron*. 2012, 27, 2325-2337

[26] Z. Wu, X. Dou, J. Chu and M. Hu, "Operation and control of a direct-driven PMSG-based wind turbine system with an auxiliary parallel grid-side converter", *Energies*, 2013, 6, 3405-3421.

[27] X. Yuan, F. Wang and D. Boroyevich, "DC-link voltage control of a full power converter for wind generator operating in weak-grid systems", *IEEE Trans. Power Electron.*, 24, pp. 2178-2192, 2009.

[28] S. Li and T. A. Haskew, "Characteristic study of vector-controlled direct driven permanent magnet synchronous generator in wind power generation", in *Proc. IEEE Power and Energy Society General Meeting - Conversion and Delivery of Electrical Energy in the 21st Century*, Pittsburgh, PA, USA, 2008.

[29] C. I. Hill, P. Zanchetta and S. V. Bozhko, "Accelerated electromechanical modeling of a distributed internal combustion engine generator unit", *Energies*, 2012, 5, 2232-2247.

[30] The CIMAC working group, "Transient response behaviour of gas engines", *Position Paper*, April 2011.

[31] A. Leitner-Audoui, M. Perktold, J. Huber and J. Thalhauser, "Highly transient load response", *29th CIMAC World Congress*, Vancouver, Canada, June 10-14, 2019.

[32] Y. Miura, S. Kokubo, D. Maekawa and T. Ise, "Efficiency improvement of a gas engine cogeneration system by power factor control with an IGBT rectifier," in *Proc. Power Conversion Conference*, Nagoya, Japan, 2-5 April 2007.

[33] M. Mueller and H. Polinder, "Electrical Drives for Direct Drive Renewable Energy Systems", Woodhead Publishing, 2013, Chap. 6.

[34] R. C. Dugan and T. E. McDermott, "Distributed generation," *IEEE Ind. Appl. Mag.*, vol. 8, no. 2, pp. 19–25, Mar./Apr. 2002.

Chapter 2
Gas Engine Generator with Energy Storage and VSG-controlled Inverter

2.1 Introduction

In this chapter, the VSG control with an additional energy storage system (ESS) is proposed for the stand-alone gas engine generator system. The overall framework of the proposed control system for a stand-alone gas-engine generator, consisting two developed control loops using the VSG concept and an electric double layer capacitor (EDLC) based energy storage system (ESS), is shown in Fig. 2.1. The design details of both control systems are discussed in this chapter. The main (open-loop) system consists of a gas engine, a permanent magnet synchronous generator (PMSG), a simple full-wave diode rectifier, a dc-link capacitor, an inverter and the load. The ESS is connected to the dc-link via a bidirectional chopper.

In this study, the capacity of ESS is calculated based on the demanded load power to deliver adequate energy during load transients. An energy-variables-based feedback control structure is adopted for the bidirectional chopper control. The control scheme of VSG is introduced and the benefit of VSG control for the stand-alone gas engine system is discussed. The transient performance of the proposed system is analyzed under sudden load change conditions by both simulation and experimental studies.

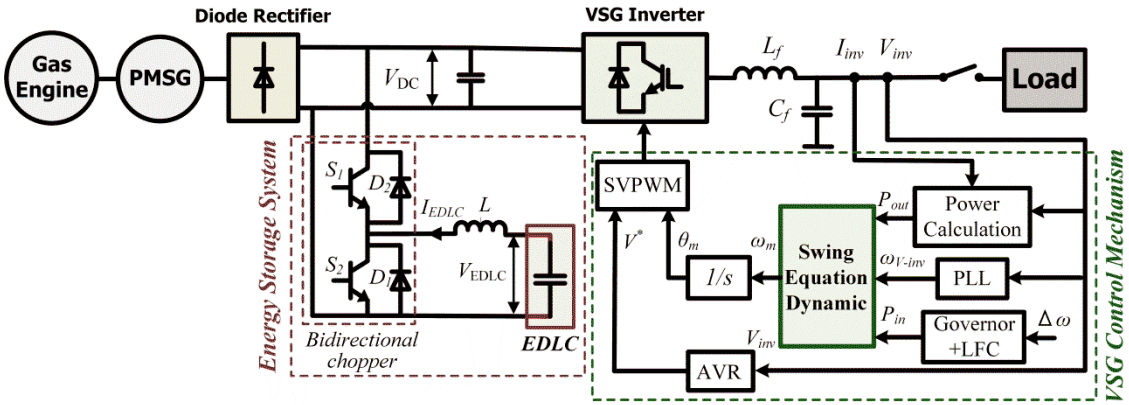

Figure 2.1 Configuration of the proposed control schemes for a gas engine generator system

2.2 VSG control scheme

The VSG control block diagram studied in this thesis is shown in Fig. 2.2. In this figure, the "Swing Equation Function" block emulates the function of swing equation of a synchronous generator as expressed in (2.1).

$$P_{in} - p_{out} = J\omega_m \frac{d\omega_m}{dt} - D\Delta\omega_m \tag{2.1}$$

where P_{in} and P_{out} are the input power and the output power, respectively; J is the inertia moment, D is the damping factor, ω_m is the virtual angular velocity of virtual rotor, $\Delta\omega_m$ is the slip between the virtual angular frequency and the frequency of inverter output voltage (ω_m - $\omega_{V\text{-}inv}$), which is used to mimic the dynamics of damper windings during transients. Here, the phase-locked loop (PLL) is used for detecting $\omega_{V\text{-}inv}$. As for stand-alone system, ω_m determines the frequency of the network and $\omega_{V\text{-}inv}$ follows ω_m.

Instead of PLL, one may use other simpler detectors. However, in the stand-alone system application, there is no need to worry about the oscillatory issues of the PLL. The PLL oscillatory dynamic mostly appeared when the PLL is used to synchronize the inverter with an external voltage source, which is not the presented case.

The values of J and D are defined in the inverter control program as the inverter does not have a rotating mass. Then, the swing equation is solved in the control program and ω_m is obtained. To solve the swing equation, the forth-order Runge-Kutta iterative algorithm is used to obtain the change of ω_m over a time step Δt. By integrating ω_m, the phase reference θ_m for the output voltage of the inverter is calculated. In the block "Power Calculation", the active power P_{out} is calculated from inverter output voltage and inverter output current by using (2.2). The line-to-line root-mean-square (RMS) value of inverter output voltage V_{inv} is calculated by using (2.3).

$$P_{out} = v_{inv\_a} i_{inv\_a} + v_{inv\_b} i_{inv\_b} + v_{inv\_c} i_{inv\_c} \tag{2.2}$$

$$V_{inv} = \sqrt{v_{inv\_a}^2 + v_{inv\_b}^2 + v_{inv\_c}^2} \tag{2.3}$$

Like a typical SG, the automatic voltage regulator (AVR) is used to regulate the actual inverter voltage V_{inv} to match the inverter base voltage V_{inv}^*. The output of AVR is the voltage magnitude reference V^* for inverter output voltage. The block diagram of AVR is shown in Fig. 2.3. A governor function can also be performed in VSG control scheme for the control of the load-power as shown in Fig. 2.4.

In this study, a simple first-order lag represents the governor function and δ is the droop coefficient in percent. However, in case of load variations, the frequency deviates

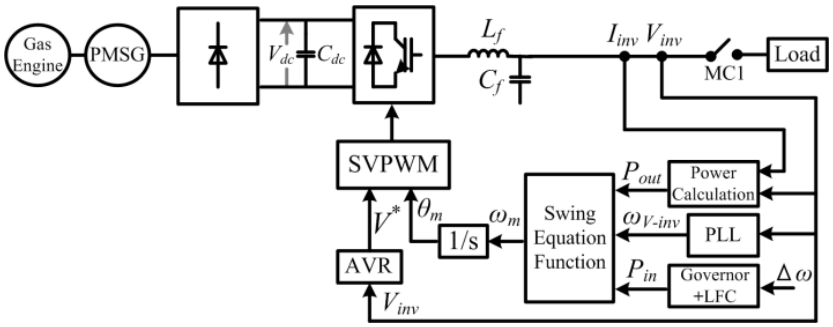

Figure 2.2 VSG Control block diagram

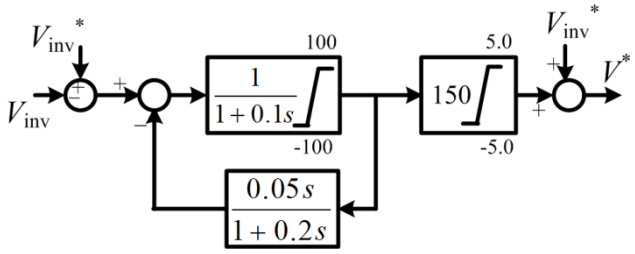

Figure 2.3 Block diagram of AVR

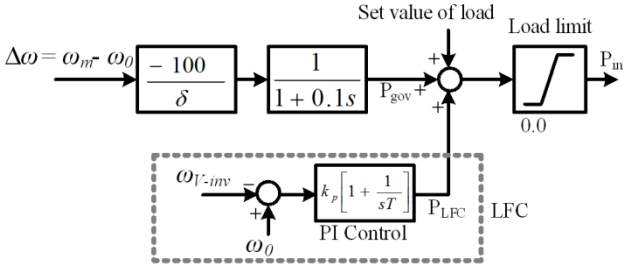

Figure 2.4 Governor and load-frequency control

from the base frequency due to the droop characteristic of governor. Therefore, the load-frequency control (LFC) is incorporated with the governor control in order to maintain the frequency at the inverter base frequency, f_{inv_0}, in case of load fluctuations. The parameters for LFC controller are presented in Table 2.2. These parameters are tuned in the simulation to obtain the proper performance of the frequency response.

2.3 Evaluation of VSG control response

In this section, the benefit of VSG control for a stand-alone gas engine is evaluated by simulation study. The evaluation is done for the load increase case. The results of system responses are compared to the results of the same system with the constant-voltage constant-frequency (CVCF) control method. The aim of this evaluation

is to analyze the characteristics of VSG control and CVCF control for stand-alone system. Therefore, an external ESS is not added to the dc link capacitor. The system configurations with the respective control scheme are shown in Fig. 2.1 and Fig. 2.5.

In the simulation study, the gas engine model is simplified by combining the engine time delay and the settling time of speed controller. Therefore, a simple PI speed controller shown in Fig. 2.6 represents the engine model. The parameters of the speed controller, the PMSG and the VSG control scheme are listed in Tables 2.1 and 2.2, respectively. These parameters are set to be close to the test result of engine speed response when the engine operates without using the ESS. For the system with CVCF control, the parameters of PI control are $k_p = 0.008$ s and $T_i = 1$, respectively.

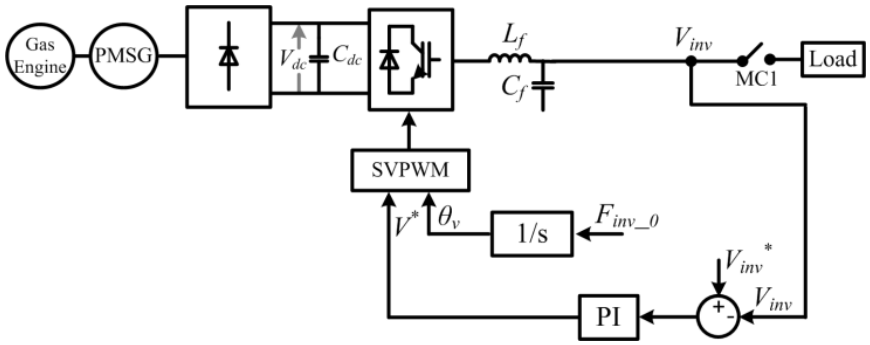

Figure 2.5 CVCF control scheme

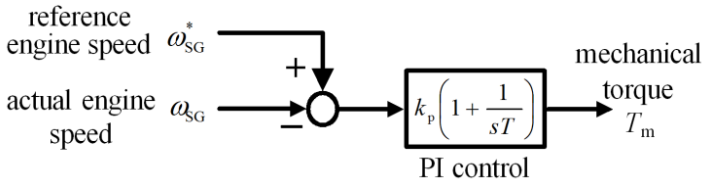

Figure 2.6 Simplified speed control block that represents gas engine

Table 2.1. Parameters of PMSG and speed controller

X_d	0.219 pu	X_q	0.219 pu
X_d'	0.027 pu	X_q'	0.027 pu
T_{do}'	6.55 s	T_{qo}'	0.85 s
X_d''	0.01 pu	X_q''	0.01 pu
T_{do}''	0.039 pu	T_{qo}''	0.071 pu
Base power	10 kW	Base voltage	210 V
Reference speed ω_{SG}^*	1710 min^{-1}	Per-unit inertia constant	0.08 s
Speed control PI gain k_{pG}	0.035	Speed control PI time constant T_G	1.0 s

Table 2.2. Parameters of VSG control

Base Power P_{base}	10 kW	Base voltage V	200 V
Base Frequency f_{inv_0}	60 Hz	Speed regulation factor δ	5 %
Per-unit inertia constant M	10 s	Inertia moment J	0.7036 kg.m^2
Damping Factor D	17 pu	Inverter switching frequency f	15 kHz
LFC PI gain	20	LFC PI time constant	0.5 s
Output voltage command V_{inv}*	200 V		

Table 2.3. Parameters of Induction Motor Load

Rated power	9 kW	Angular speed	377 rad/s
Rated volatge	200 V	Per-unit inertia constant M	10 s
Rated current	26 A		

As the gas engine is operating in the stand-alone mode, the effect of VSG control is more obvious in the case of frequency dependent load compared to the case of frequency independent load. Therefore, in order to make clear the advantage of VSG over CVCF control, the frequency dependent load, an induction motor is used for both the cases. The parameters of induction motor load are shown in Table 2.3.

The simulations are performed for both the systems under the step loading condition. The simulation results of engine speed and generator output power against a sudden load-power increase are shown in Fig. 2.7.

Before 20 s, the system is running with no load and the engine speed is maintained at its rated speed of 1710 min^{-1}. At 20 s, the load is connected to the system and the engine speed decreases suddenly in both cases as shown in Fig. 2.7 (a). In both cases, the speed recovers to its rated value after 2 s. However, the amount of speed dip under VSG control is nearly 80 min^{-1} smaller than the case with CVCF control. Moreover, there are some oscillations in the engine speed waveform of the case with CVCF control while there are no oscillations in the waveform of the case with VSG control.

The simulation results of generator output power for both cases are shown in Fig. 2.7 (b). At the start of loading, there are a small overshoot and some oscillations in the waveform of the case with CVCF control. In case of VSG control, the power changes in a smooth way at the instant of loading. These simulation results show that the engine speed variations and generator output power changes can be properly damped by using the VSG control due to the effect of virtual inertia.

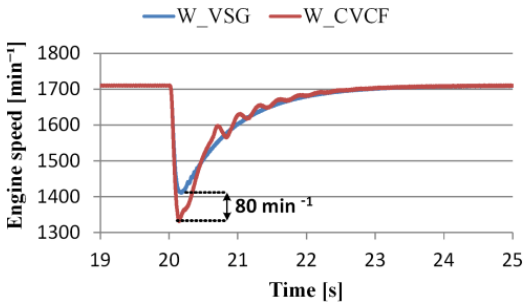

(a)

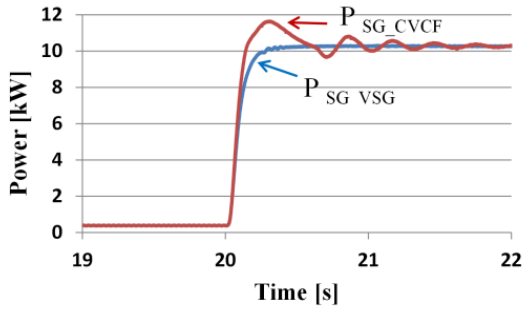

(b)

Figure 2.7 Simulation results of loading case comparing VSG control and CVCF control (a) Engine speed, (b) Generator output power for loading case

Therefore, the proposed VSG control for the stand-alone operation of gas engine generator provides an improved transient performance.

2.4 Energy storage system control structure

The ESS is connected to the dc-link of the system. As mentioned, the purpose of this study is to improve the characteristics of the gas engine generator under transient conditions, and therefore it is necessary to supply energy in a short time. The EDLC has the characteristics that it can send a large amount of energy in a short time. For this reason, the EDLC is used as an energy storage device in this study.

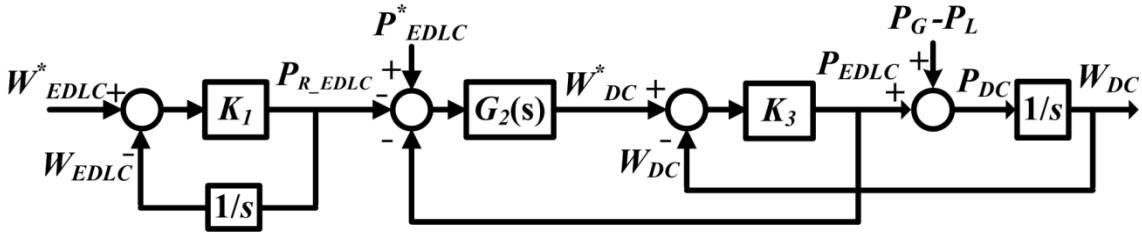

Figure 2.8 Feedback control structure for energy storage

For both loading and load removal cases, the energy of EDLC should be recovered to the original amount level after the system has reached to its steady state. Therefore, an energy-variables-based feedback control strategy is proposed for controlling energy transfer between EDLC and dc link as shown in Fig. 2.8. In Fig. 2.8, the proposed control structure is composed of three control loops.

In the energy recovery control loop, the actual EDLC energy W_{EDLC} is compared with the reference W^*_{EDLC} and the error is sent to a proportional controller. The output of proportional controller is the recovery power of EDLC $P_{\mathrm{R\_EDLC}}$ and sent to the EDLC power control loop. In the EDLC power control loop, P^*_{EDLC} is the reference EDLC power. The error of P_{EDLC} is the input to a PI controller, and the output of PI controller is the reference value for the dc-link energy control. In the dc-link energy control loop, W^*_{DC} is the reference dc-link energy and W_{DC} is the actual dc-link energy. The error of W_{DC} is sent to a proportional controller and the output of the controller is the EDLC power P_{EDLC}.

In this control structure, the design of time constants is the key point and thus in the following subsections, the settings of time constants are explained.

2.4.1 dc-link energy control

The control loop of dc-link energy control can be illustrated as shown in Fig. 2.9. In this diagram, P_G is the generator output power, P_L is the load power, P_{DC} is the dc-link power, K_3 is the gain and s is the Laplace operator.

$$\begin{aligned} &\left(W^*_{DC} - W_{DC}\right)\frac{K_3}{s} = W_{DC} \\ &\Leftrightarrow \frac{K_3}{s}W^*_{DC} = W_{DC}\left(1+\frac{K_3}{s}\right) \end{aligned} \tag{2.4}$$

From (2.4), the transfer function for the dc-link energy control is derived as in (2.5).

$$\frac{W_{DC}}{W^*_{DC}} = \frac{\dfrac{K_3}{s}}{1+\dfrac{K_3}{s}} = \frac{1}{1+\dfrac{1}{K_3}s} = \frac{1}{1+sT_3} \tag{2.5}$$

where the time constant is expressed as in (2.6).

$$T_3 = \frac{1}{K_3} \tag{2.6}$$

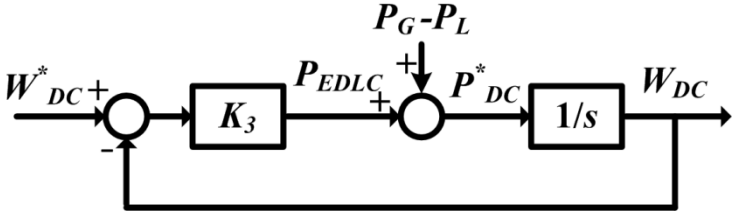

Figure 2.9 dc-link energy control block diagram

2.4.2 EDLC power control

The control loop diagram for EDLC power control is shown in Fig. 2.10. From Fig. 2.10, the transfer function of EDLC power control loop can be written as follows:

$$\left(W_{DC}^{*} - W_{DC}\right)K_3 = P_{EDLC} \tag{2.7}$$

$$\left(P_{EDLC}^{*} - P_{EDLC}\right)G_2(s) = W_{DC}^{*} \tag{2.8}$$

In steady state, P^{*}_{EDLC} is zero. By substituting (2.8) into (2.7), the following relationship can be obtained

$$\begin{aligned} &\left(-G_2(s)P_{EDLC} - W_{DC}\right)K_3 = P_{EDLC} \\ &\Leftrightarrow -W_{DC}K_3 = P_{EDLC}\left(1 + G_2(s)K_3\right) \end{aligned} \tag{2.9}$$

and

$$P_{EDLC} = -\frac{K_3}{1 + G_2(s)K_3}W_{DC} \tag{2.10}$$

When $G_2(s) = K_p\,(1+1/sT_2)$, where K_p is a proportional gain and T_2 is an integral time constant, (2.10) can be rewritten as (2.11).

$$P_{EDLC} = -\frac{sT_2K_3}{K_3K_p + s\left(1 + K_3K_p\right)T_2}W_{DC} \tag{2.11}$$

If W_{DC} in (2.11) is considered as a unit step input, P_{EDLC} becomes

$$\begin{aligned} P_{EDLC} &= -\frac{sT_2K_3}{K_3K_p + s\left(1 + K_3K_p\right)T_2}\frac{1}{s} \\ &= \frac{-\dfrac{K_3}{\left(1 + K_3K_p\right)}}{s + \dfrac{K_3K_p}{\left(1 + K_3K_p\right)T_2}} \end{aligned} \tag{2.12}$$

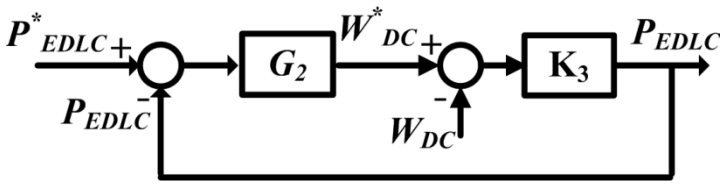

Figure 2.10 *EDLC* power control block diagram

Finally, using inverse Laplace transform, the unit step response of P_{EDLC} can be obtained as follows.

$$P_{EDLC} = -\frac{K_3}{(1+K_3K_p)}\exp\left\{-\frac{K_3K_p}{(1+K_3K_p)T_2}t\right\} \tag{2.13}$$

2.4.3 EDLC energy recovery control

The EDLC energy recovery control loop is shown in Fig. 2.11. The time constant T_1 of this control loop is derived as follows:

$$\begin{aligned} &\left(W^*_{EDLC} - W_{EDLC}\right)\frac{K_1}{s} = W_{EDLC} \\ &\Leftrightarrow \frac{K_1}{s}W^*_{EDLC} = W_{EDLC}\left(1+\frac{K_1}{s}\right) \end{aligned} \tag{2.14}$$

where K_1 is the proportional gain.

From (2.14), the transfer function for EDLC energy control is obtained as given in (2.15).

$$\frac{W_{EDLC}}{W^*_{EDLC}} = \frac{\frac{K_1}{s}}{1+\frac{K_1}{s}} = \frac{1}{1+\frac{1}{K_1}s} = \frac{1}{1+sT_1} \tag{2.15}$$

where the time constant is expressed as

$$T_1 = \frac{1}{K_1} \tag{2.16}$$

The time constant of each control loop is derived as explained above. Among the three control loops, the fastest response is required for the dc link energy W_{DC} control loop. The slowest response is for the EDLC energy recovery control loop. Therefore, T_1 should be sufficiently larger than T_3. And, T_2 value should be placed between T_1 and T_3. Moreover, the response speed of EDLC power control loop determines how much disturbance the energy storage system absorbs.

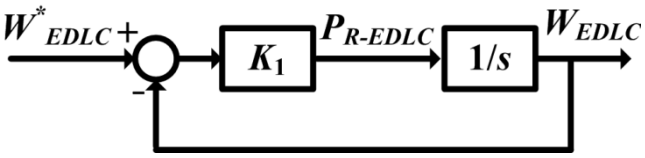

Figure 2.11 EDLC energy recovery control block diagram

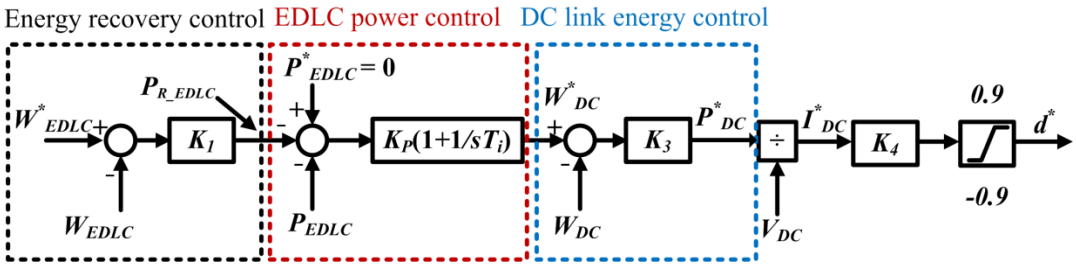

Figure 2.12 Overall control block diagram of ESS

If the response speed is too fast, the power of energy storage will not appear because the EDLC power is zero in steady state. Based on these assumptions, the time constants are determined as $T_1 = 20$ s, $T_2 = 4$s, and $T_3 = 0.01$s in order to satisfy $T_1 > T_2 > T_3$. The corresponding values of gains are obtained as $K_1 = 1/T_1 = 0.05$ and $K_3 = 1/T_3 = 100$. The proportional gain of EDLC power controller is set as $K_p = 0.01$.

From the above mentioned feedback control scheme, the overall control diagram can be represented as shown in Fig. 2.12. In Fig. 2.12, the output of dc link energy control loop is the current signal. Therefore, the gain K_4 is used to convert from the dimension of current signal (ampere) to the duty command d^*.

2.4.4 Stability analysis of ESS control loop

The feedback control structure of ESS was presented in Fig. 2.12. In Fig. 2.12, the EDLC power controller and the dc link energy control are the main control loops for the control of ESS. The EDLC energy recovery control loop is an additional control loop for recovering the energy to its steady state after transient period. Therefore, only the main control loops are considered in the stability and performance analysis of closed-loop system and the transfer function of P^*_{EDLC} to W_{DC} is obtained as follows:

$$\frac{W_{DC}}{P^*_{EDLC}} = \frac{(K_3K_pT_2)s + K_3K_p}{(K_3K_pT_2)s^2 + (K_3T_2 + K_3K_p)s} \tag{2.17}$$

Using (2.17), the root locus diagrams of closed-loop transfer function for each control parameter are described in Fig. 2.13. The characteristic equation includes two roots on the real axis. One is located at the origin, which is fixed, and does not influence by changing the three parameters. However, the second root is highly dependent to the

parameters selection. As shown in Fig. 2.13, the poles are remained on the left-half plane for a wide range of each parameter variation. However, the performance and stability margin may be affected by selecting different values. As shown in Fig. 2.13, the parameters T_2, K_p and K_3 have been selected such that the stability and performance of the control system are not degraded.

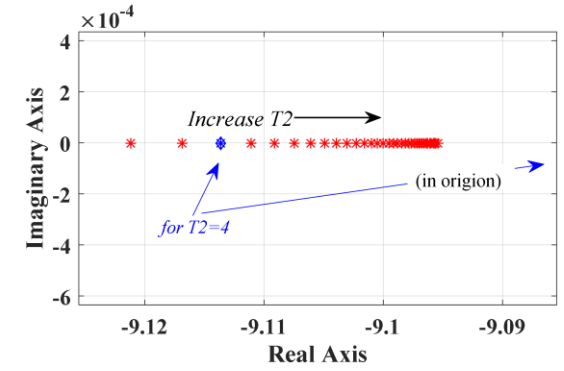

(a)

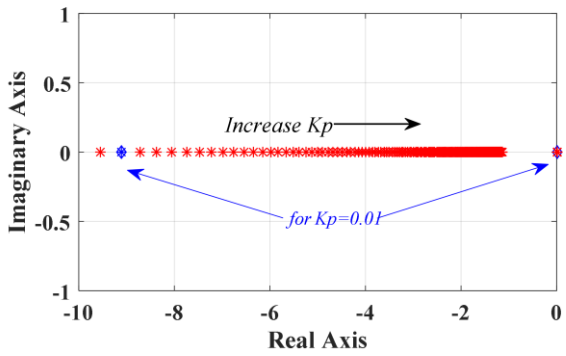

(b)

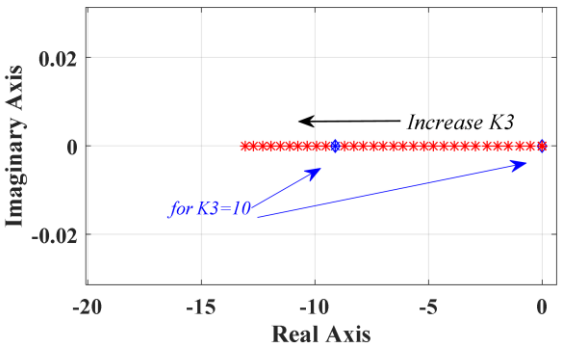

(c)

Figure 2.13 The root locus diagrams of the ESS closed-loop system (a) T_2 varies from 0.01 to 10, (b) K_p varies from 0.05 to 1 , (c) K_3 varies from 1 to 1200

2.4.5 Generation of switching signals of bidirectional chopper

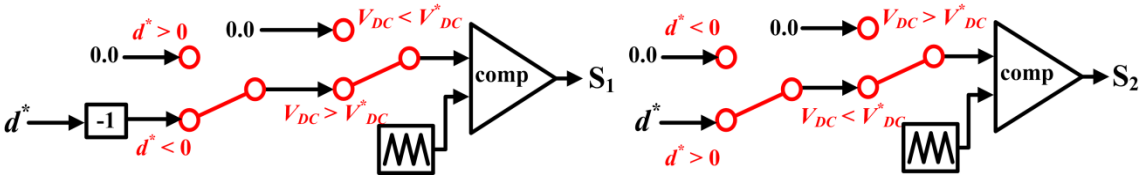

Figure 2.14 Scheme of switching signals generation

The switching signals for the bidirectional chopper are generated as shown in Fig. 2.14. In Fig. 2.14, S_1 and S_2 are the upper and lower switching signals of the chopper, V^*_{DC} is the reference dc link voltage, V_{DC} is the actual dc-link voltage, d^* is the duty cycle. The reference dc-link voltage V^*_{DC} is calculated from the reference dc-link energy W^*_{DC}. As illustrated in the figure, the sign of the duty cycle d^* indicates the operation mode of bidirectional chopper; negative sign for the buck mode and positive sign for the boost mode. In the buck mode, V_{DC} is greater than V^*_{DC} and the EDLC charges power from the dc-link. In the boost mode, V_{DC} is less than V^*_{DC} and the EDLC discharges power to the dc-link.

2.5 Calculation of energy storage capacity

In order to calculate the required capacity of energy storage, the load change is assumed to be in a step shape as shown in Fig. 2.15. In Fig. 2.15, P_{LOAD} is load power, P_{gen} is engine generator output power and τ_g is a generator time constant. As can be seen in the figure, P_{gen} responds to the step change of P_{LOAD} with delay.

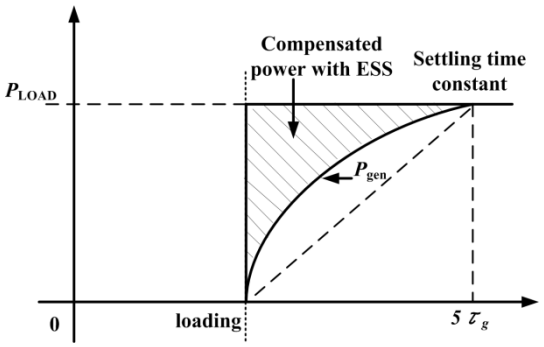

Figure 2.15 Step load power response of generator

The incremental difference between the load power and generator output power is considered as the kinetic energy of rotor which causes variations in rotational speed of engine generator. The rotational speed variations of engine generator can be suppressed if the kinetic energy of rotor is compensated by using the ESS. Based on this assumption, the capacity of energy storage can be calculated as the following procedures.

2.5.1 Calculating kinetic energy of rotor

As shown in Fig. 2.15, the kinetic energy of rotor for step load change can be calculated by using τ_g because the rotational speed response depends on τ_g. The speed approximately returns to its steady state after $5\tau_g$ under the assumption that the change is approximated as an exponential curve. Thus, it can be considered that the kinetic energy of rotor is generated during this period of $5\tau_g$. For simplicity, the kinetic energy is calculated by assuming in a triangular area as shown in Fig. 2.15. If the values of τ_g and the rated load power P_{LOAD} are known, the kinetic energy of rotor can be calculated as given in (2.18). In this study, the value of τ_g is set as 1 s and P_{LOAD} is 10 kW, and therefore the required energy W is calculated as

$$W = \frac{1}{2} \times P_{LOAD} \times 5\tau_g = 25000\,[\mathrm{J}] \tag{2.18}$$

The obtained kinetic energy is considered as the required amount of energy to be compensated by the ESS.

2.5.2 Calculating maximum voltage limit of EDLCs system

When Space Vector PWM is adopted, the maximum dc-link voltage V_{DC} can be determined according to the generator rated voltage $V_{AC\text{-}RMS}$ as

$$V_{DC} = \sqrt{2}\, V_{AC-RMS} \tag{2.19}$$

In this work, the value of $V_{AC\text{-}RMS}$ is fixed at 210 V. Thus, the calculated V_{DC} is 297 V. The maximum EDLC voltage limit V_{max} should be less than V_{DC} because the boost chopper is connected between the EDLC and dc link. Therefore, V_{max} is chosen as 200 V, and the minimum EDLC voltage limit V_{min} is chosen as 100 V (50 percent of V_{max}). Then, in order to calculate the stand-by energy, the stand-by voltage V_0 can be calculated by using the capacitor energy equation. Separating charging and discharging cases, only half of total energy is used to calculate V_0 as

$$\frac{1}{2}CV_0^2 = \left(\frac{1}{2}CV_{max}^2 + \frac{1}{2}CV_{min}^2\right) \times \frac{1}{2} \tag{2.20}$$

$$V_0 = \sqrt{\frac{V_{\min}^2 + V_{\max}^2}{2}} \tag{2.21}$$

Substituting the values of $V_{\max}$ and $V_{\min}$, the value of V_0 is obtained as 160 V. Using V_0 and $V_{\min}$, the total capacitance of EDLC C_{tot} can be calculated as

$$C_{tot} = \frac{2W}{\left(V_0^2 - V_{\min}^2\right)} \tag{2.22}$$

By the above equation, C_{tot} of EDLC is calculated as 3.5 F.

2.5.3 Calculating minimum number of EDLC units

The value of $V_{\max}$ is used for determining the number of EDLC units for series connection. For practical applications, the rating of EDLC voltage should be greater than the maximum EDLC voltage limit $V_{\max}$. In this study, the rating of EDLC voltage is set as 1.25 times of $V_{\max}$. Then, the number of EDLC units for series connection n_s can be expressed as

$$n_s = \frac{1.25 \times V_{\max}}{v_1} \tag{2.23}$$

Here, v_1 is the rated voltage of one EDLC. In this study, $V_{\max}$ is 200 V and v_1 is 2.5 V, then n_s = 100. When 100 EDLC units with 350 F for each EDLC are connected in series, the total capacitance is 3.5 F which is matched with C_{tot}, the calculated total capacitance of EDLC.

2.6 Simulation results

The circuit diagram illustrated in Fig. 2.1 is used in simulation. In order to verify the performance of the proposed control scheme, simulations are carried out for two cases of with EDLC and without EDLC.

The transient responses of closed-loop system are investigated under both load connection and load removal conditions. For both cases, at 90 s, the load is connected to or disconnected from the system. For the 10 kW base power of the system, the step responses are analyzed by using a 9-kW (0.9 pu) resistive load. The parameters of PMSG and VSG control were listed in Table 2.1 and Table 2.3 in section 2.3. The parameters of ESS control are listed in Table 2.4.

First, the results of loading case are presented. In Fig. 2.16, the engine speed response to load connection is depicted. In Fig. 2.16(a), the engine speed decreases from its rated value of 1710 min^{-1} to 1450 min^{-1}. In Fig. 2.16(b), the engine speed decreases

from 1710 min^{-1} to 1610 min^{-1}. Therefore, the speed dip due to loading is reduced by 160 min^{-1} using EDLC.

Table 2.4. Parameters of Energy Storage System

Minimum EDLC voltage, V_{min}	100 V	Maximum EDLC voltage, V_{max}	200 V
Stand-by voltage of EDLC, V_0	160 V	Gain, k_4	100
Gain of W_{DC}^* control k_3	1000	Total capacitance of EDLC	3.5 F
Gain of P_{EDLC} control, k_p	0.01	Time constant of P_{EDLC} control, T_2	2 s
Gain of recovery control, W_{EDLC} ,k_1	0.08	Chopper switching frequency, f	15 kHz
Reactor inductance, L	0.39 mH		

The dc-link voltage response is shown in Fig. 2.17. Before the load is connected, the value of dc-link voltage is 390 V for both cases. The dc-link voltage drops to 300 V at the start of loading in the case of without EDLC. After that, it returns back to around 320 V. With EDLC, the dc-link voltage firstly drops to about 340 V, and then it gradually decreases to around 320 V. The waveforms in Fig. 2.17 show that the dc-link voltage has a smooth change in the case of using EDLC.

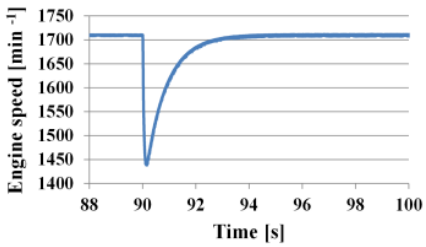

(a) without EDLC

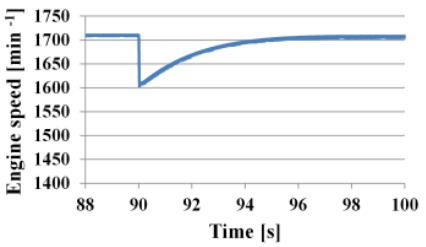

(b) with EDLC

Figure 2.16 Engine speed response to load connection

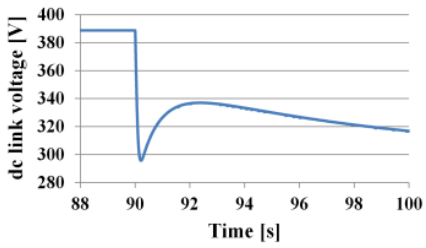

(a) without EDLC

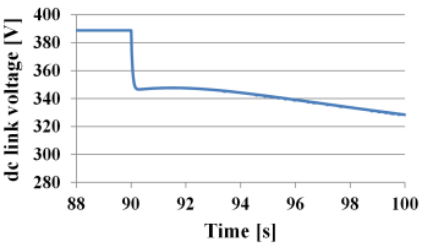

(b) with EDLC

Figure 2.17 dc-link voltage response to load connection

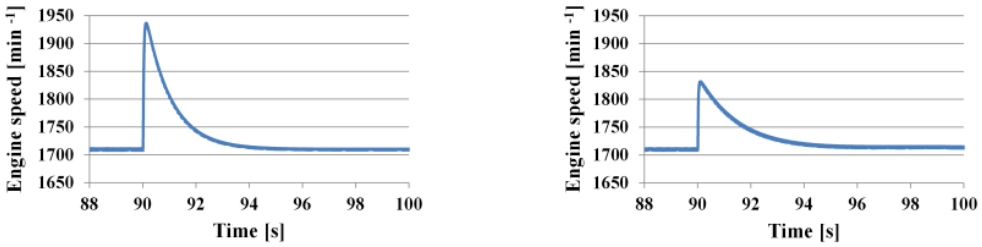

(a) without EDLC (b) with EDLC

Figure 2.18 Engine speed response to load removal condition

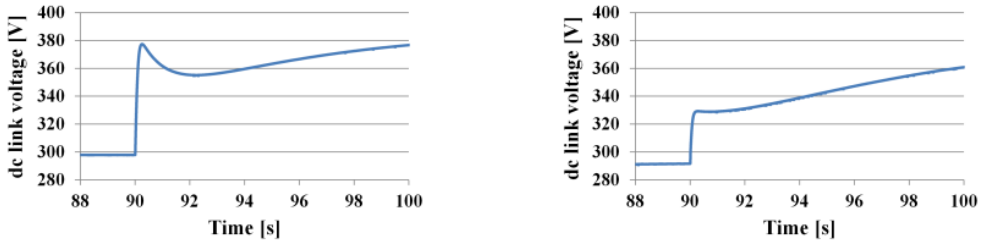

(a) without EDLC (b) with EDLC

Figure 2.19 dc link voltage response to load removal condition

The engine speed and dc voltage for load removal case are illustrated in Figs. 2.18 and 2.19, respectively. Fig. 2.18(a) shows that the engine speed increases from 1710 min^{-1} to 1940 min^{-1} when the load is removed from the system. In Fig. 2.18(b), the engine speed increases from 1710 min^{-1} to 1830 min^{-1}. These results show that the speed rise is reduced by 110 min^{-1} using EDLC.

In Fig. 2.19(a), there is a small overshoot in dc voltage when the load is removed from the system. In Fig. 2.19(b), the dc-link voltage has small overshoot and returns back to its steady state value after the load is removed from the system.

In Fig. 2.20, the reactor current of EDLC is shown. In the load connection case, the positive current indicates that the EDLC energy is transferred to the dc-link. At the instant of loading, the current rises to 80 A, and decreases to get back zero state after transient. For the load removal case, the negative current indicates that the EDLC absorbs power from the dc-link. The current decreases to -60 A when the load is removed from the system. After transient period, it is returned to reach the zero state. From the waveforms of EDLC voltage and current, it is confirmed that the bidirectional chopper works well in the boost mode for the loading case, and in the buck mode for the load removal case.

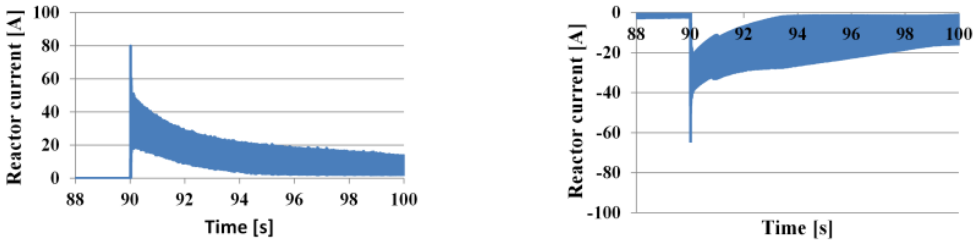

(a) Load connection case (b) Load removal case

Figure 2.20 EDLC current response to load transient

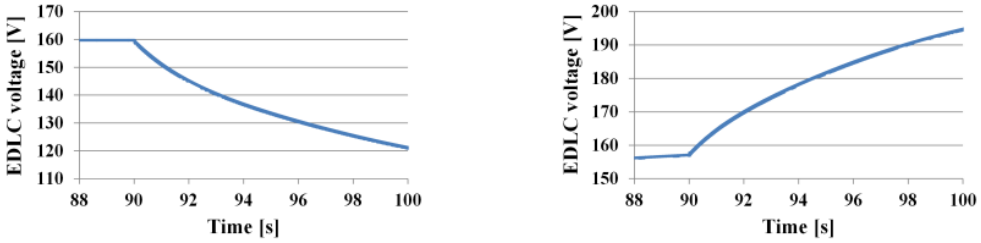

(a) Load connection case (b) Load removal case

Figure 2.21 EDLC voltage response to load transient

Fig. 2.21 shows the EDLC voltage waveforms of both the loading and load removal cases. The EDLC voltage decreases from its stand-by voltage of 160 V to 120 V in the load connection case, and the voltage increases from its stand-by voltage to nearly 195 V in the case of load removal.

By using the EDLC voltage variations, the delivered energy and the absorbed energy of ESS can be calculated. The delivered energy for the load connection case can be calculated as

$$W = \frac{1}{2} C \times \left(160^2 - 120^2\right) = 19600 \ [\mathrm{J}]$$

The absorbed energy for the load removal case can be calculated as

$$W = \frac{1}{2} C \times \left(195^2 - 158^2\right) = 22857 \ [\mathrm{J}]$$

From these calculation results, the amount of energy for both load connection and load removal cases are within the amount of estimated energy in section 2.5.1.

2.7 Experimental results

An experimental study was conducted in order to verify the effectiveness of the proposed control system. The experimental circuit diagram is shown in Fig. 2.22. The real engine generator set of model number CP10VB1Z manufactured by Yanmar Company was used in the experiment.

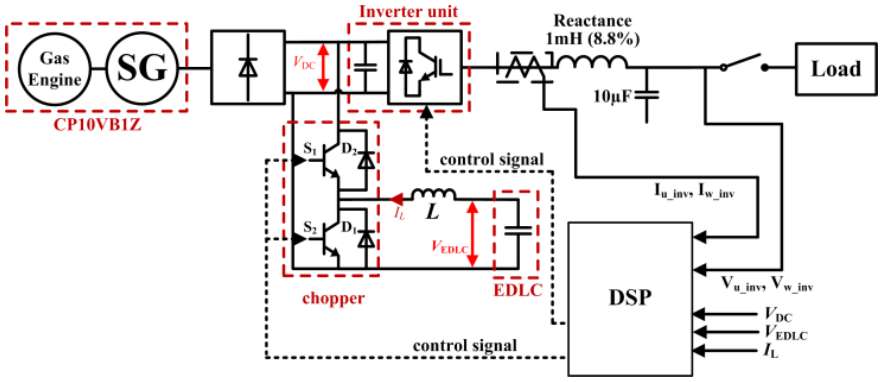

Figure 2.22 Experimental circuit configuration with real engine set

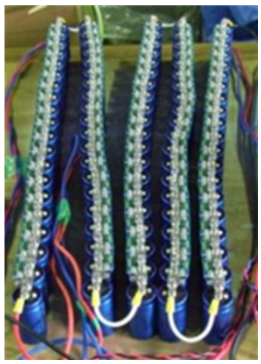

Figure 2.23 Configuration of EDLC

The system operation conditions for the experiment were the same as those explained in the simulation study. The parameters of PMSG, VSG controller and ESS control were also the same as assumed in the simulation study. As presented in section 2.5, the ESS used in experimental study is composed of 100 units of EDLCs connected in series. The rated voltage of each EDLC is 2.5 V. The total capacitance of energy storage is 3.5 F. The configuration of EDLC used in experiment is shown in Fig. 2.23.

The variations of engine speed for the load connection case are shown in Fig. 2.24. In Fig. 2.24(a), without EDLC, the engine speed decreased from its rated value of 1710 min^{-1} to 1450 min^{-1}. In Fig. 2.24(b), with EDLC, the engine speed decreased from 1710 min^{-1} to 1550 min^{-1}. Therefore, the engine speed deviation was reduced 100 min^{-1} by

using the EDLC. In Fig. 2.25, before connecting the load, the value of dc-link voltage was kept at 390 V for both the cases. When the load was connected to the system without the EDLC, the dc-link voltage suddenly decreased to 260 V and then returned to nearly 300 V, whereas in the case with the EDLC, the dc voltage gradually decreased to 300 V.

The results of load removal case are shown in Figs. 2.26 and 2.27, respectively. In Fig. 2.26(a), at the time of load disconnection, the engine speed rose to 2000 min^{-1} at first, and then it decreased continuously because the engine operation stopped. It shows that the engine speed variation exceeded its maximum allowable limit. However, under the operation with EDLC, the speed rose to 1800 min^{-1} and the system maintained in operation as shown in Fig. 2.26(b).

In Fig. 2.27(a), the dc-link voltage rose to nearly 470 V when the load was removed from the system because the operation broke down. In Fig. 2.27(b), the dc-link voltage returned to its steady state value of 390 V after removing the load from the system.

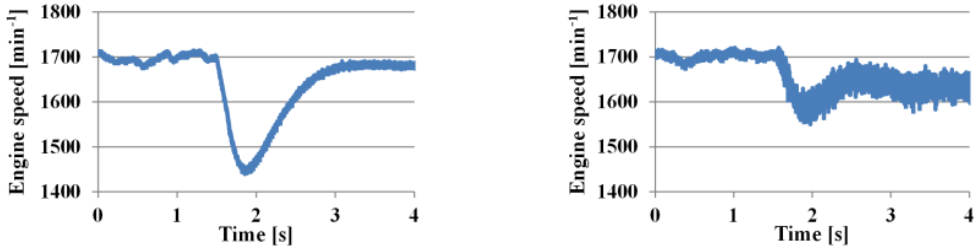

(a) without EDLC (b) with EDLC

Figure 2.24 Engine speed response to load connection (Experiment)

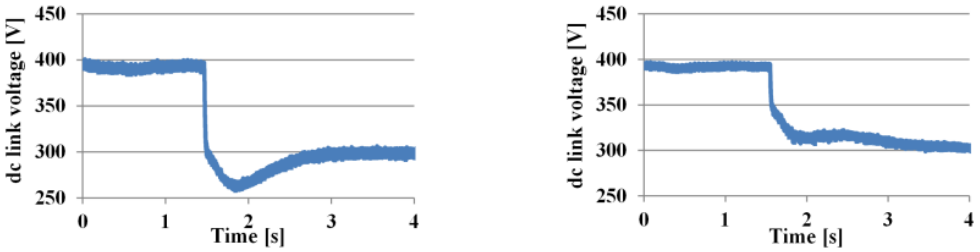

(a) without EDLC (b) with EDLC

Figure 2.25 dc-link voltage response to load connection (Experiment)

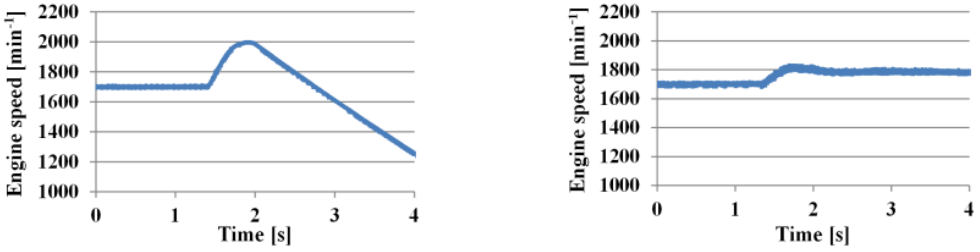

(a) without EDLC (b) with EDLC

Figure 2.26 Engine speed response to load removal (Experiment)

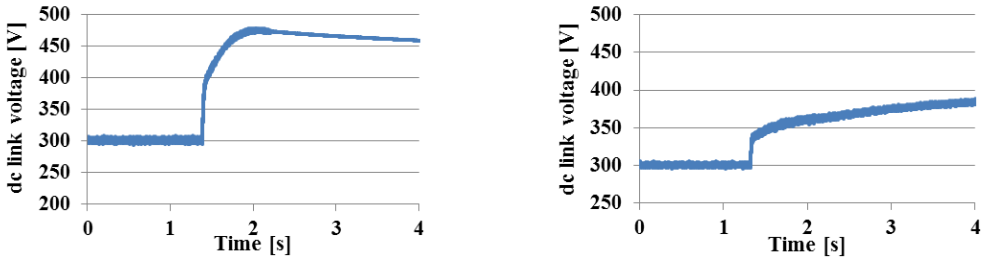

(a) without EDLC (b) with EDLC

Figure 2.27 dc-link voltage response to load removal (Experiment)

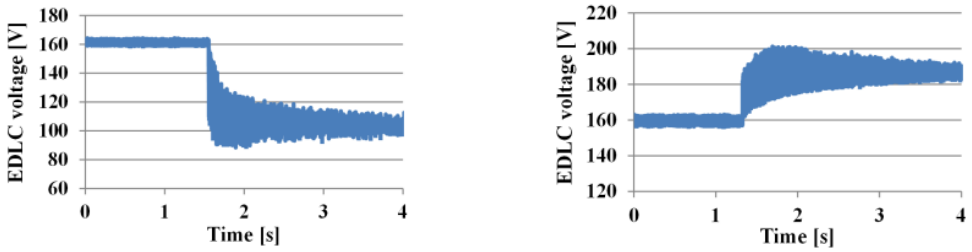

(a) Load connection case (b) Load removal case

Figure 2.28 EDLC voltage response to load transient (Experiment)

The results of measured EDLC voltages are shown in Fig. 2.28. For load connection case, the EDLC voltage dropped from its stand by voltage of 160 V to nearly 100 V (minimum limit) as the energy storage is providing power to the dc-link. In the case of load removal, the EDLC voltage is increased from 160 V to nearly 195 V, which means the EDLC was charged from the dc-link. There are some ripples in the waveforms of EDLC voltage. These ripples are due to the saturation of inductor in the ESS system.

In the same way as simulation study, the delivered energy for the loading case can be calculated as

$$W = \frac{1}{2} C \times \left(160^2 - 102^2\right) = 26593\,[\mathrm{J}]$$

The absorbed energy for the load removal case can be calculated as

$$W = \frac{1}{2} C \times \left(188^2 - 160^2\right) = 17052 \text{ [J]}$$

From experimental results, the amount of energy for load connection case is almost close to the amount of estimated energy. The amount of energy for load removal case is within the amount of estimated energy in section 2.5.

Table 2.5. Speed Variations in Ratio for 9 kW Load

Loading	**Simulation**	**Experiment**
Without EDLC	Decrease 260 min^{-1} (15.2% of rated speed)	Decrease 260 min^{-1} (15.2% of rated speed)
With EDLC	Decrease 90 min^{-1} (5.3% of rated speed)	Decrease 160 min^{-1} (9.4% of rated speed)

Since the main aim of this study is to reduce gas-engine speed variations under sudden load changes, the results of speed deviations under load transients are summarized in Table 2.5. The results of loading cases prove that the proposed control scheme can significantly reduce gas-engine speed deviations by adding an external ESS to the dc-link that connected with VSG control.

2.8 Summary

In order to improve the transient performance of stand-alone gas engine generator at the instant of sudden load change, the VSG control method in combination with an external ESS is proposed in this paper. The dynamic characteristics of the proposed gas engine generator system were investigated under load connection and load removal cases for the 0.9 pu load step change. The investigations were done by both simulation and experimental studies.

The obtained simulation and experimental results verified that the proposed control structure compensated the slow response of engine's mechanical system by providing a temporary energy during transient state. As a result, the engine speed variations were well suppressed and the system was operating without shutting down for the 0.9 pu load step change. Therefore, the proposed control scheme can improve the transient characteristics of stand-alone gas engine generator system.

References

[1] Rosli Abu Bakar Semin, “A technical review of compressed natural gas as an alternative fuel for internal combustion engines,” *American Journal of Engineering and Applied Sciences 1 (4)*, pp. 302-311, 2008.

[2] ヤンマー株式会社 HP ：マイクロコージェネレーションシステム　CP シリーズ　スペック-主要仕様一覧

[3] http://www.yanmar.co.jp/energy/products/microCogeneration/cp/spec.html#anchor07

[4] G. Iwanski and W. Koczara, “Power management in an autonomous adjustable speed large power diesel gensets,” in *Proc. EPE-PEMC Power Electronics and Motion Control Conf.*, 2008, Poznan, pp.2164-2169.

[5] A. Mondal, A. A. Renjit, M. S. Illindala and J. H. Eto, “Operation and impact of energy storage system in an industrial microgrid”, in *Proc. 2015 IEEE Industry Applications Society Annual Meeting*, Addison, TX, USA, 18-22 Oct. 2015.

[6] J.h. Lee, S. H. Lee and D. K. Sul, “Variable-speed engine generator with supercapacitor: isolated power generation system and fuel efficiency”, *IEEE Trans. Ind. Appl.*, Vol.45, no.6, pp.2130-2135, Nov/Dec.2009.

[7] T. Hikihara, T. Sawada, T. Funaki, “Enhanced entrainment of synchronous inverters for distributed power sources”, *IEICE Trans. on Fundamentals*, vol.E90-A, No. 11, November 2007.

[8] G. Delille, B. François and G. Malarange, “Dynamic frequency control support by energy storage to reduce the impact of wind and solar generation on isolated power system’s inertia”, *IEEE Trans. Sustainable Energy*, vol. 3, no. 4, pp.931-939, Oct. 2012.

[9] V. S. K. M. Balijepalli, A. Ukil, N. Karthikeyan, A. K. Gupta, Y. Shicong, “Virtual synchronous generators as potential solution for electricity grid compliance studies,” *2016 IEEE Region 10 Conference*, 22-25 Nov. 2016.

[10] T. Shintai, Y. Miura, and T. Ise, “Oscillation damping of a distributed generator using a virtual synchronous generator,” *IEEE Trans. Power Delivery*, vol. 29, no. 2, pp. 668–676, April 2014.

[11] J. Liu, Y. Miura, and T. Ise, “Comparison of dynamic characteristics between virtual synchronous generator and droop control in inverter-based distributed generators”, *IEEE Trans. Power Electron.*, vol. 31, no. 5, pp. 3600–3611, May 2016.

[12] Y. Hirase, K. Sugimoto, K. Sakimoto and T. Ise, “Analysis of resonance in microgrids and effects of system frequency stabilization using a virtual

synchronous generator," *IEEE J. Emerg. Sel. Topics Power Electron.*, vol. 4, no. 4, pp. 1287–1298, Dec. 2016.

[13] J. Liu, Y. Miura, and T. Ise, "Fixed-parameter damping methods of virtual synchronous generator control using state feedback," *IEEE Access*, vol. 7, pp. 99177–99190, 2019.

[14] J. A. Suul, S. D'Arco, and G. Guidi, "Virtual synchronous machine-based control of a single-phase bi-directional battery charger for providing vehicle-to-grid services," *IEEE Trans. Ind. Appl.*, vol. 52, no. 4, pp. 3234–3244, July–Aug. 2016.

[15] M. A. Torres L., L. A. C. Lopes, Luis A. Moran T. and Jose R. Espinoza C, "Self-tuning virtual synchronous machine: A control strategy for energy storage systems to support dynamic frequency control", *IEEE Trans. Energy Conv.*, vol. 29, no. 4, pp. 833–840, December 2014.

[16] D. Li, Q. Zhu, S. Lin and X.Y. Bian, "A self-adaptive inertia and damping combination control of VSG to support frequency stability", *IEEE Trans. Energy Conv.*, vol. 32, no. 1, pp. 397–398, March 2017.

[17] J. Fang, Y. Tang, H. Li and X. Li, "A bttery/ultracapacitor hybrid energy storage system for implementing the power management of virtual synchronous generators", *IEEE Trans. Power Electron.*, vol. 33, no. 4, pp. 2820–2824, April 2018.

[18] T. H. Nguyen and D. C. Lee, "Ride-through technique for PMSG wind turbines using energy storage systems," *Journal of Power Electronics*, Vol. 10, No. 6, pp. 733-738, November 2010.

[19] Z. Wu, D. W. Gao, H. Zhang, S. Yan, and X. Wang, "Coordinated control strategy of battery energy storage system and PMSG-WTG to enhance system frequency regulation capability", *IEEE Trans. Sustainable Energy*, Vol. 8, No. 3, pp. 1330-1343, JULY 2017.

[20] Y. Tan, K. M. Muttaqi, P. Ciufo, L. Meegahapola, X. Guo, B. Chen, and H. Chen, "Enhanced frequency regulation using multilevel energy storage in remote area power supply systems", *IEEE Trans. Power System*, Vol. 34, No. 1, pp. 163-170, Jan. 2019.

[21] M. N. Musarrat, M. R. Islam, K. M. Muttaqi, and D. Sutanto, "Enhanced frequency support from a PMSG-based wind energy conversion system integrated with a high temperature SMES in standalone power supply systems", *IEEE Trans. Appl. Superconductivity*, Vol. 29, No. 2, pp. 3800206-3800206, MARCH 2019.

Chapter 3
Gas Engine Generator with Active Rectifier and VSG-controlled Inverter

3.1 Introduction

In this chapter, a fully controllable frequency converter is employed in the PMSG based gas engine generator system which is operated in stand-alone mode. A general view of the system is depicted in Fig. 3.1. The whole system includes of an engine, a surface mounted PMSG, a back-to-back power converter consisting of two insulated gate bipolar transistors (IGBT)-based ac-dc converters and a dc-link, and a load. This study is performed with two main objectives. The first one is to improve the generator output stator current waveform by using an active rectifier instead of a diode rectifier. The second is to support a smooth power transition during load changes by applying the VSG control on the load side converter.

The overall proposed system with mentioned control loops, i.e. active rectifier control and VSG control can be seen in Fig. 3.1. The VSG control scheme explained in chapter 2 is applied for the control of load side converter. The mathematical model of a PMSG and the constant stator voltage (CSV) control method for the generator side converter will be presented in this chapter. The system responses are studied under loading and load removal cases in PSCAD software environment. The simulation results of the system with a diode rectifier and with the proposed active rectifier are discussed.

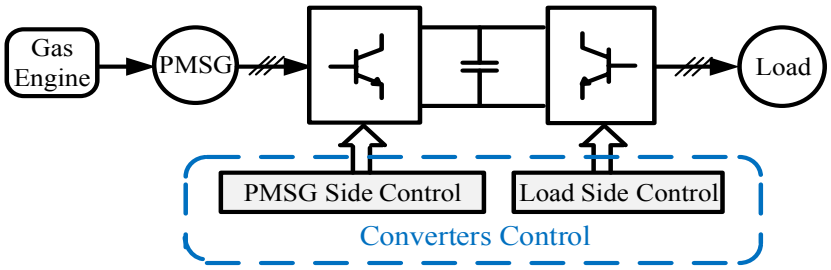

Figure 3.1. Overall structure of the gas engine generator system

3.2 PMSG dynamic model

In the dq-coordinates of rotor reference frame, assuming the magnetic flux is aligned with the d-axis, the dynamic model of the surface mounted PMSG can be represented as in (3.1), where ψ_m is the flux linkage of the permanent magnet, R_s is the stator resistance,

ω_e is the rotor speed in electrical degree, v_{ds} , v_{qs}, i_{ds} ,i_{qs} , L_{ds} and L_{qs} are the d- and q-components of the stator voltage, current and inductance.

$$\begin{bmatrix} v_{ds} \\ v_{qs} \end{bmatrix} = -R_s \begin{bmatrix} i_{ds} \\ i_{qs} \end{bmatrix} - \frac{d}{dt} \begin{bmatrix} L_{ds} i_{ds} \\ L_{qs} i_{qs} \end{bmatrix} + \omega_e \begin{bmatrix} -L_{qs} i_{qs} \\ L_{ds} i_{qs} + \psi_m \end{bmatrix} \tag{3.1}$$

Under the steady-state condition, (3.1) can be expressed as

$$\begin{bmatrix} v_{ds} \\ v_{qs} \end{bmatrix} = \begin{bmatrix} -R_s & -\omega_e L_{qs} \\ \omega_e L_{ds} & -R_s \end{bmatrix} \begin{bmatrix} i_{ds} \\ i_{qs} \end{bmatrix} + \begin{bmatrix} 0 \\ \omega_e \psi_m \end{bmatrix} \tag{3.2}$$

For a surface mounted type PMSG, the electromagnetic torque, active power and reactive power can be expressed as

$$T_e = \frac{3}{2} p \psi_m i_{qs} \tag{3.3}$$

$$P_s = v_{ds} i_{ds} + v_{qs} i_{qs} \tag{3.4}$$

$$Q_s = v_{qs} i_{ds} - v_{ds} i_{qs} \tag{3.5}$$

where p is the number of pole pairs. From the above mathematical expressions of surface mounted PMSG, the PMSG side converter can be controlled in various schemes based on vector control methods to achieve the different control objectives. The general idea of vector control is to use the ac flux based reference frame or the ac voltage based reference frame for extending the currents in the reference frame. The extended currents become dc quantities and are referred to as the d and q components of the respective currents. The voltage based reference frame is 90° ahead of the flux based reference frame. In the voltage based reference frame, the active power aligns on the d-component and the reactive power is on the q-component. The positions are opposite in the flux based reference frame.

3.2.1 Description of reference frames

The phasor diagram of PMSG vectors in the reference frames is illustrated in Fig. 3.2. In Fig. 3.2, the voltage based reference is termed as stator voltage reference frame (SVRF) and the flux based reference frames are termed as stator flux reference frame (SFRF) and rotor reference frame (RRF).

(a) Stator voltage reference frame (SVRF)

The SVRF rotates with the angular speed of the stator voltage. In this frame, the stator voltage vector is on the d-component. Thus, the stator voltage U_s has only the d-component voltage v_{ds} which implies that the d-axis current corresponds to the active power and the q-axis current corresponds to the reactive power.

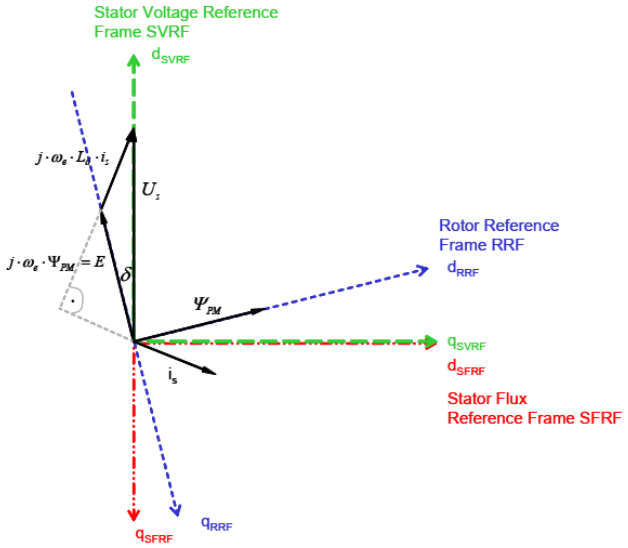

Figure 3.2. Phasor diagram of PMSG illustrating the reference frames [18]

(b) Stator flux reference frame (SFRF)

The SFRF is perpendicular to the SVRF, i.e, the stator flux is perpendicular to the stator voltage. This frame also rotates with the angular speed of the stator voltage. In this frame, the rotor flux superposes on the stator flux.

(c) Rotor reference frame (RRF)

The RRF rotates with the angular speed of rotor flux. In this frame, the induced voltage *E* which is on q-axis is perpendicular to the rotor flux vector that is on d-axis. Thus, the active power corresponds to the q-axis and the reactive power corresponds to the d-axis.

3.3 Control scheme of PMSG side converter

In PMSG, the induced voltage cannot be controlled as the excitation comes from the permanent magnet. Therefore, the induced voltage is proportional to the generator speed and varies with the speed. In the case of over-speed, the overvoltage occurs in the generator and converter. To overcome this problem, in this study, the constant stator voltage (CSV) control method is adopted for the control of PMSG side converter and the detailed control scheme are explained in the following subsection.

In this control scheme, the generator output stator voltage is controlled by controlling the stator current. The control structure is implemented in the stator voltage reference frame (SVRF) where the stator voltage vector is aligned on the d-axis and the stator voltage on q-axis is equal to zero. Thus, the active power and reactive power of PMSG become

$$P_s = v_{ds} i_{ds} \tag{3.6}$$

$$Q_s = -v_{ds} i_{qs} \tag{3.7}$$

From (3.6) and (3.7), the active power depends on the stator d-axis current and the reactive power depends on the q-axis stator current. Again, the relationship between the ac input power and dc output power of the converter can be expressed as

$$P_s = v_{ds} i_{ds} = P_{dc} = v_{dc} i_{dc} \tag{3.8}$$

where v_{dc} and i_{dc} are the dc-link voltage and current. Hence, instead of the active power, the dc-link voltage v_{dc} can be controlled by the the stator d-axis current. Moreover, instead of the reactive power, the stator voltage can be controlled by the stator q-axis current. The block diagram of the overall control structure with the CSV control in the Active Rectifier Control block is shown in Fig. 3.3. The VSG control scheme shown in the VSG Control block is well discussed in Chapter 2. In this figure, the PMSG side converter control is a cascaded control with an inner current controller and an outer voltage controller on the d- and q-axes. Hence, it consists of four proportional integral (PI) controllers in which PI 1 is the dc-link voltage controller, PI 2 is the stator voltage controller, PI 3 and PI 4 are the d- and q-axis current controllers.

In dc-link voltage control, the reference dc-link voltage V_{dc}^* and the actual measured voltage V_{dc} are compared and the error is sent to PI 1. The output of PI 1 is the reference d-axis current i_{ds}^*. Then, i_{ds}^* is compared with the actual measured value i_{ds} and the error is sent to PI 3. The output of PI 3 is the reference voltage signal e_d^* to the converter.

In the stator voltage control loop, the reference stator voltage V_{gen}^* is compared with the actual stator voltage V_{gen} which is calculated from the generator output voltage as in (3.9). Then, the error is sent to PI 2.

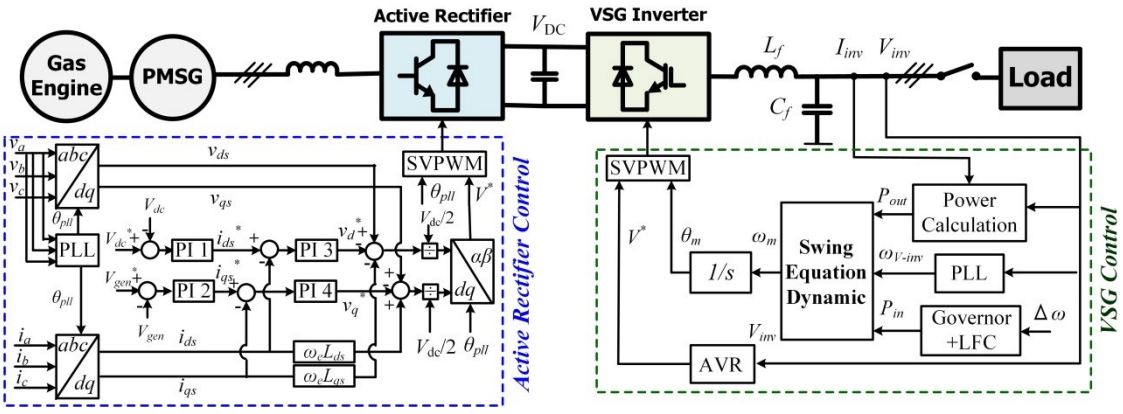

Figure 3.3. CSV control scheme for the PMSG side converter

The output of PI 2 is the reference q-axis current i_{qs}^*. Then, i_{qs}^* is compared with the actual measured value i_{qs} and the error is sent to PI 4. The output of PI 4 is the reference voltage signal e_q^* to the converter.

$$V_{\text{gen}} = \sqrt{v_{ds}^2 + v_{qs}^2} \tag{3.9}$$

After adding the decoupling terms $\omega_e L i_{ds}$, $\omega_e L i_{qs}$ and the feed forward terms v_{ds}, v_{qs} to the e_d^* and e_q^*, these voltages are transformed into $\alpha\beta$ values to calculate the reference voltage V^* for space vector pulse width modulation (SVPWM). The park transformation method is used to transform the measured three-phase voltages and currents into two-phase voltages and currents in d-q co-coordinate system. As the control scheme is in the stator voltage-oriented reference frame, the required voltage angle θ_{PLL} for dq-transformation is detected by the phase lock loop (PLL) circuit. Therefore, an encoder is not necessary in this control method. The proposed generator side control will be compared with two well-known other controlled methodologies named zero d-axis current (ZDC) control, unity power factor (UPF) control in chapter 4.

3.3.1 Inner current controller

The inner current controller is designed based on the relationship between generator output voltage and the rectifier input voltage as shown in equation (3.10).

$$\begin{bmatrix} v_a \\ v_b \\ v_c \end{bmatrix} = L\frac{d}{dt}\begin{bmatrix} i_a \\ i_b \\ i_c \end{bmatrix} + \begin{bmatrix} e_a \\ e_b \\ e_c \end{bmatrix} \tag{3.10}$$

Here, v_a, v_b, v_c are generator terminal voltages; i_a, i_b, i_c are generator output currents; and e_a, e_b, e_c are converter voltages, for the phases a, b and c respectively. L is the inductance between generator terminal and rectifier. Equation (3.10) can be transformed into dq frame using the Park transformation, the following equations are achieved:

$$\begin{bmatrix} v_{ds} \\ v_{qs} \end{bmatrix} = R_s\begin{bmatrix} i_{ds} \\ i_{qs} \end{bmatrix} + L\frac{d}{dt}\begin{bmatrix} i_{ds} \\ i_{qs} \end{bmatrix} + \omega_e L\begin{bmatrix} -i_{qs} \\ i_{ds} \end{bmatrix} + \begin{bmatrix} e_d \\ e_q \end{bmatrix} \tag{3.11}$$

$$v_{ds} - e_d = R_s i_{ds} + L\frac{d}{dt}i_{ds} - \omega_e L i_{qs} \tag{3.12}$$

$$v_{qs} - e_q = R_s i_{qs} + L\frac{d}{dt}i_{qs} + \omega_e L i_{ds} \tag{3.13}$$

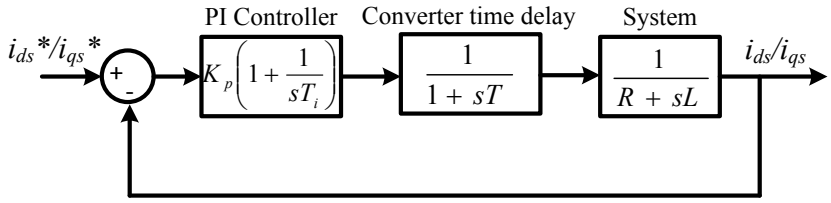

Figure 3.4. Block diagram of inner current controller

Equations (3.12) and (3.13) are dependent on both d-axis and q-axis currents. In order to decouple the two axes, an adopted voltage for controller output is defined as follow.

$$u_d^* = R_s i_{ds} + v_{ds} - e_d + \omega_e L i_{qs} \tag{3.14}$$

$$u_q^* = R_s i_{qs} + v_{qs} - e_q - \omega_e L i_{ds} \tag{3.15}$$

where, v_{ds} and v_{qs} are the feedforward terms, $\omega_e L i_{ds}$ and $\omega_e L i_{qs}$ are decoupling terms for the controller, in here, $L = L_{ds} = L_{qs}$. Hence, due to the feedforward terms, the control system allows the d- and q- axes to be decoupled and independent.

By rearranging (3.14) and inserting the result to (3.12), and doing the similar process with (3.15) and (3.13), we obtain equations (3.16) and (3.17), which provide the system transfer function of the controller.

$$u_d^* = R_s i_{ds} + L\frac{d}{dt} i_{ds} \tag{3.16}$$

$$u_q^* = R_s i_{qs} + L\frac{d}{dt} i_{qs} \tag{3.17}$$

As seen from (3.16) and (3.17), the equations in d-axis and q-axis have a similar form. Using Laplace transform and considering the converter as an ideal power transformer with a time delay, the block diagram of inner current controller is obtained as shown in Fig. 3.4.

3.3.2 Outer dc-link voltage controller

The block diagram of dc voltage controller is shown in Fig. 3.5.The current balance of the dc-link, as described in equations (3.18) and (3.19) are considered for voltage controller design.

$$i_{cap} = i_{dc} - i_L \tag{3.18}$$

$$C\frac{d}{dt} v_{dc} = \frac{v_d}{v_{dc}} i_{ds} - i_L \tag{3.19}$$

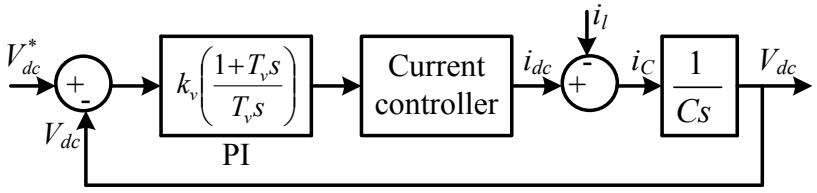

Fig. 3.5 DC voltage controller structure

This dc-link current equation is a non-linear equation. It is necessary to linearize the system model around the operating point and then perform linear stability analysis. It can be done by applying Taylor series expansion of non-linear function around the steady state reference point. In this case, if we consider i_L as a disturbance and the ratio of v_d and v_{dc} as constant values, the linear expression becomes

$$C\frac{d\Delta v_{dc}}{dt} = \Delta i_{ds} \tag{3.20}$$

Using Laplace transformation, (3.20) is transferred to (3.21).

$$\frac{\Delta v_{dc}}{\Delta i_{ds}} = \frac{1}{sC} \tag{3.21}$$

3.4 Simulation-based comparison between diode rectifier and IGBT rectifier

Several simulations are performed to examine the response of the proposed control framework in the PSCAD/EMTDC software environment. To show the effectiveness of using an IGBT rectifier, simulations are carried out for two different system topologies for the generator side converter: with a diode rectifier and with an IGBT rectifier. Similar parameters are used for both systems because the IGBT-based rectifier acts as a full-bridge diode rectifier under the gate-blocking condition owing to the connected diodes to the IGBTs in an anti-parallel configuration. For both cases, the load side converter is controlled by the VSG control method.

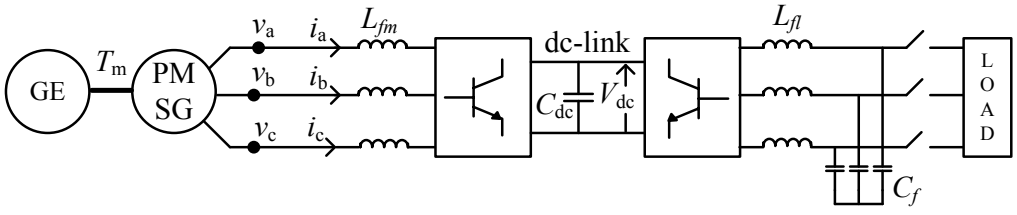

Figure 3.6 Circuit configuration used in the simulations

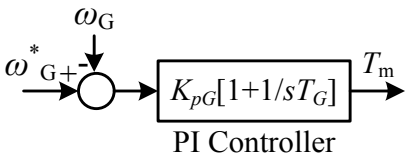

Figure 3.7 Speed controller of the gas engine

The simulations are performed for the system shown in Fig. 3.6. In the simulation study, the gas engine model is simplified by combining the engine time delay and the settling time of speed controller. Therefore, a simple PI speed controller shown in Fig. 3.7 represents the engine model. The parameters of the speed controller, the PMSG and the VSG control scheme are listed in Tables 3.1 and 3.2, respectively. The circuit parameters and the PI control parameters are listed in Table 3.3.

The total simulation time is fixed at 20 s. The generator is initialized to run at a speed of 1710 min^{-1} without load. After 3 s, a resistive load of 40 ohm which is equivalent to a 0.5 pu load (1kW) is connected to the system and the system response to the step load change from 0 kW to 1 kW is analyzed. At 15 s, the load is removed from the system and the system response to the step load change from 1 kW to 0 kW is investigated.

Table 3.1. Parameters of the PMSG

X_d	0.219 pu	X_q	0.219 pu
X_d'	0.027 pu	X_q'	0.027 pu
T_{do}'	6.55 s	T_{qo}'	0.85 s
X_d''	0.01 pu	X_q''	0.01 pu
T_{do}''	0.039 pu	T_{qo}''	0.071 pu
Base power	2 kW	Base voltage	200 V
Engine speed command ω_{SG}^*	1710 min^{-1}	Per-unit inertia constant	0.08 s
Speed control PI gain k_{pG}	0.035	Speed control PI time constant T_G	1.0 s

Table 3.2. Parameters of the VSG control

Base Power P_{base}	10 kW	Base voltage V	200 V
Base Frequency f_{inv_0}	60 Hz	Speed regulation factor δ	5 %
Per-unit inertia constant M	10 s	Inertia moment J	0.7036 kg.m^2
Damping Factor D	17 pu	Switching frequency f_s	15 kHz
LFC PI gain	20	LFC PI time constant	0.5 s
Inverter reference voltage V_{inv}^*	200 V		

Table 3.3. Circuit parameters and PI control parameters

L_{fm}	2 mH	L_{fl}	1 mH
C_{dc}	4.7 mF	C_{fl}	10 μF
V_{dc}^*	400 V	V_{gen}^*	200 V
K_p of PI 1	0.3	K_p of PI 3	50
T_i of PI 1	5	T_i of PI 3	0.01
K_p of PI 2	0.1	K_p of PI 4	0.3
T_i of PI 2	1	T_i of PI 4	0.01

First, the simulation results of generator stator current waveforms in steady state are shown in Fig. 3.8. As can be seen in Fig. 3.8, the current waveform with the diode rectifier is not sinusoidal and contains large harmonic contents that can deteriorate the generator efficiency. The current waveform with the IGBT rectifier is very close to a sinusoidal waveform and the harmonic components are greatly reduced.

The engine speed response to the step loading case is shown in Fig. 3.9(a). With the diode rectifier, there is a speed dip of 110 min^{-1} due to the applied load. However, after 3 s, the speed can catch its reference value. With the IGBT rectifier, when the load is connected to the system, there is a speed decrease of 90 min^{-1}, about 20 min^{-1} smaller than that of the diode rectifier case. After 2 s, the speed can catch its reference value, properly. In Fig. 3.9(b), the engine speed response to the load removal case is shown and the engine speed variations in the case of diode rectifier are larger than the variations of the IGBT rectifier case. For both loading and load removal cases, the recovery time in the case of diode rectifier to reach its steady state is also longer than that of the IGBT rectifier case.

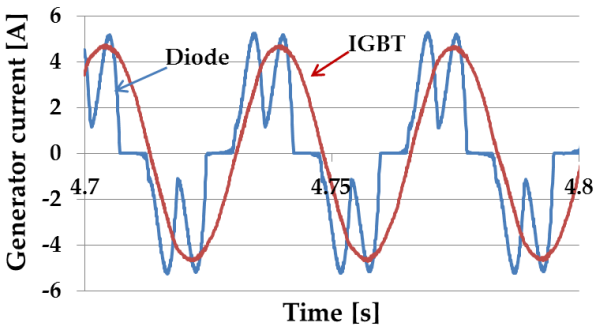

Figure 3.8. Waveforms of the generator stator current in steady state (phase a)

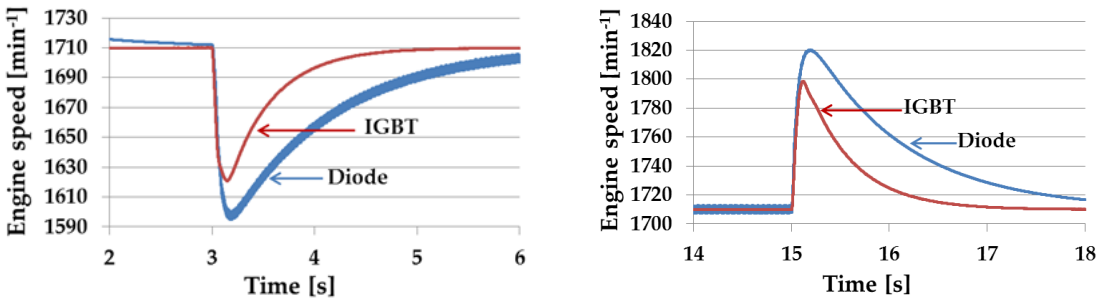

(a) (b)

Figure 3.9. The engine speed (a) loading case, (b) load removal case

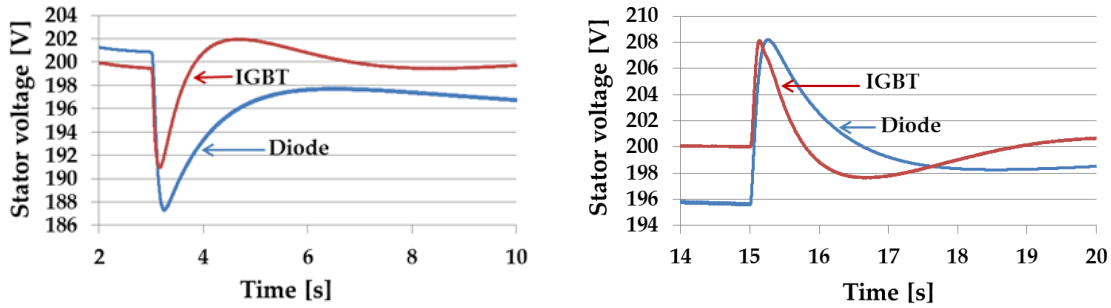

(a) (b)

Figure 3.10. The stator voltage (a) loading case, (b) load removal case

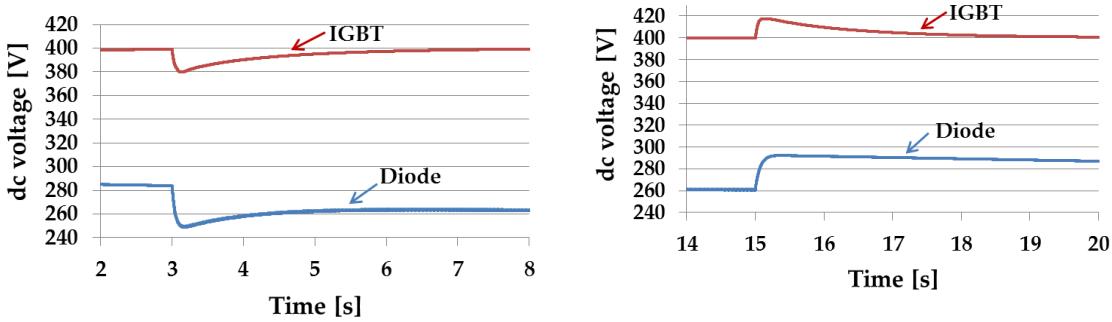

(a) (b)

Figure 3.11. The dc-link voltage (a) loading case, (b) load removal case

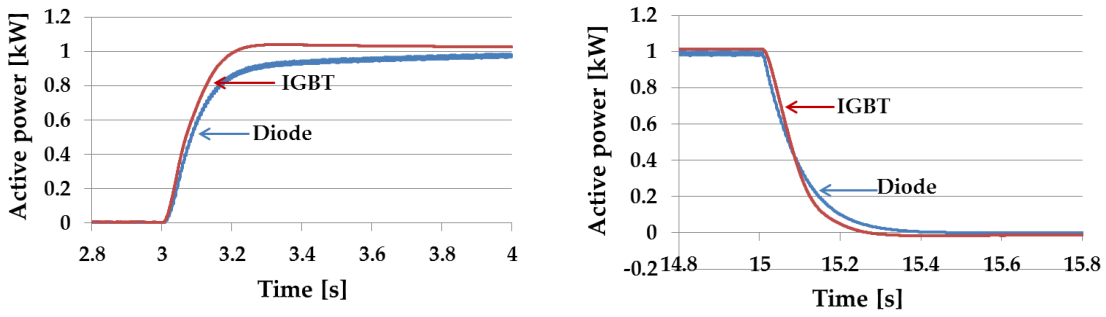

(a) (b)

Figure 3.12. The generator output active power (a) loading case, (b) load removal case

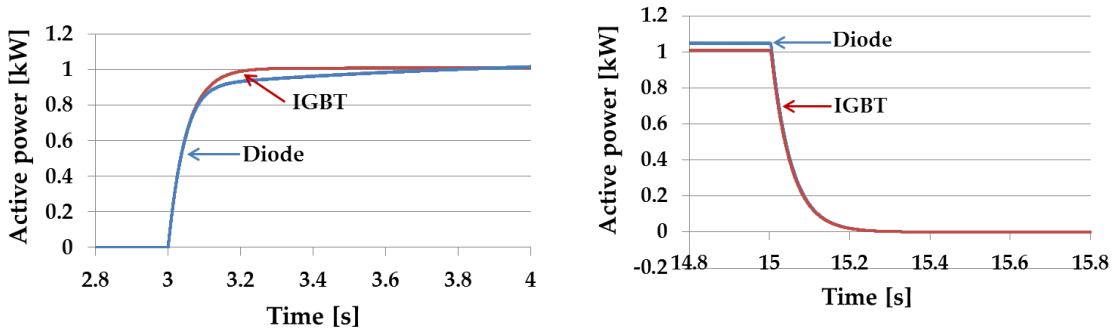

(a) (b)

Figure 3.13. The inverter output active power (a) loading case, (b) load removal case

The generator stator voltage result for the loading case is shown in Fig. 3.10(a). With the diode rectifier, at the start of loading, the stator voltage decreases from its rated voltage of 200 V to 187 V, and then recovers to 196 V at steady state. With the IGBT rectifier, at the instant of loading, the stator voltage drops to 191 V. After 2 s, the stator voltage can catch its reference value of 200 V despite of a small overshoot. For the load removal case, as can be seen in Fig. 3.10(b), the stator voltage in the case of IGBT rectifier reaches to its reference value after load transients. With the diode rectifier, the stator voltage has a small deviation from its rated value of 200 V under steady state condition. Therefore, the waveforms in Fig. 3.10 show the usefulness of stator voltage controller.

The dc-link voltage responses to loading case are shown in Fig. 3.11(a). With the diode rectifier, it can be seen that there is a significant voltage drop of 40 V at the start of loading. Moreover, the dc-link voltage is maintained at around 260 V at steady state, and cannot reach to its no-load condition value of 290 V as there is no control for both the generator field voltage and the dc-link. With the IGBT rectifier, the amount of

voltage drop at the start of load connection is about 20 V, and then the dc voltage reaches its reference value after 3 s without overshoot and steady state error.

Fig. 3.11(b) shows the dc-link voltage response to the load removal case. With the diode rectifier, the dc-link voltage recovers to its no-load condition value of 290 V when the load is removed from the system. With the IGBT rectifier, the dc-link voltage rises from 400 V to 420 V when the load is removed from the system. After 2 s, it drops to its reference value. For both the loading and the load removal cases, the results show the usefulness of dc-link voltage controller. As the IGBT rectifier is a boost type converter, the dc-link voltage with the IGBT rectifier is higher than that with the diode rectifier and can sufficiently provide the demanded load power.

The generator output active power responses are shown in Fig. 3.12. The waveforms of inverter output active power are shown in Fig. 3.13. In Fig. 3.12 and Fig. 3.13, with the diode rectifier, the settling time to reach the demanded load power is slower than that of the IGBT rectifier case. Nevertheless, in both cases, the power transitions have a smooth change during load transients owing to the effect of virtual inertia provided by the VSG control in load side converter.

Despite the mentioned benefits and advantages, like all existing control systems, the proposed control scheme may suffer from some potential problems and shortages. The main week points in practical applications can be summarized as:

(a) It is difficult to effectively use the developed control structure for the power generation systems which are unable to control the dc-link from the generator side. Because, the dc-link voltage control has to be performed by the generator side, and the VSG control method used in the inverter side cannot provide a dc-link voltage control.

(b) In comparison of diode-based rectifier, the design of proposed active rectifier is more complex, and costly. Therefore, from the economical point of view, it may not be recommended.

3.5 Summary

This chapter mainly addresses the entire control of gas engine generation system using a PMSG and a fully controllable frequency converter. In the present work, the control methodologies for the generator side and the load side converters are performed. Using the proposed control strategy, the active and reactive powers of the generator are controlled independently. For the generator side converter, the generator output active power is controlled through a dc-link voltage control loop, whereas the reactive power is controlled through the generator stator voltage controller.

For the sake of showing the effectiveness of the proposed control scheme, several computer simulations are performed for the step load change test while the generator

unit is working in stand-alone operation mode. In comparison with a diode rectifier-based system, the applied control scheme is significantly effective regarding generator current harmonic reduction. Thus, an improvement in generator efficiency can be expected. Moreover, the recovery time of engine speed after load increasing and decreasing can be much improved and the dc-link voltage can be kept higher by using the IGBT rectifier.

References

[1] B. Wu, Y. Lang, N. Zargari, and S. Kouro, “Power Conversion and Control of Wind Energy Systems”, Wiley-IEEE, USA: NJ, 2011.

[2] S. H. Qazi and M. W. B. Mustafa, “Technical issues on integration of wind farms with power grid-A review”, *International Journal of Renewable and Sustainable Energy*, 2014, 3, 87-91.

[3] Y. C. Chang, H. C. Chang and C. Y. Huang, “Design and implementation of the permanent magnet synchronous generator drive in wind generation systems”, *Energies*, 2018, 11, 1634.

[4] A. C. Barmpatza and J. C. Kappatou, “Finite element method investigation and loss estimation of a permanent magnet synchronous generator feeding a non-linear load”, *Energies*, 2018, 11, 3404.

[5] C. K. Lai, Y. Ting T. and C. C. Tsai, “Modeling, analysis, and realization of permanent magnet synchronous motor current vector control by MATLAB/Simulink and FPGA”, *Machines*, 2017, 5, 26.

[6] R. Tiwari, S. Padmanaban and R. B. Neelakandan, “Coordinated control strategies for a permanent magnet synchronous generator based wind energy conversion system”, *Energies*, 2017, 10, 1493.

[7] M. E. Haque, M. Negnevitsky and K. M. Muttaqi, “A novel control strategy for a variable-speed wind turbine with a permanent-magnet synchronous generator”, *IEEE Trans. Ind. Appl*. 2010, 46, 331-339.

[8] M. Chinchilla, S. Arnaltes and J. C. Burgos, “Control of permanent-magnet generators applied to variable-speed wind energy systems connected to the grid”, *IEEE Trans. Energy Convers*, vol. 21, pp.130-135, 2006.

[9] G. Buticchi, E. Lorenzani, F. Immovilli and C. Bianchini, “Active rectifier with integrated system control for microwind power systems”, *IEEE Trans. Sustainable Energy*. 2015. 6, 60-69.

[10] S. Li, T. A. Haskew, R. P. Swatloski and W. Gathings, “Optimal and direct-current vector control of direct-driven PMSG wind turbines”, *IEEE Trans. Power Electron*. vol. 27, pp. 2325-2337, 2012.

[11] Z. Wu , X. Dou, J. Chu and M. Hu, “Operation and control of a direct-driven PMSG-based wind turbine system with an auxiliary parallel grid-side converter”, *Energies*, 2013, 6, 3405-3421.

[12] X. Yuan, F. Wang and D. Boroyevich, “DC-link voltage control of a full power converter for wind generator operating in weak-grid systems”, *IEEE Trans. Power Electron*. 2009, 24, 2178-2192.

[13] S. Li and T. A. Haskew, “Characteristic study of vector-controlled direct driven permanent magnet synchronous generator in wind power generation” in *Proc. IEEE Power and Energy Society General Meeting - Conversion and Delivery of Electrical Energy in the 21st Century*, Pittsburgh, PA, USA, 2008.

[14] C. I. Hill, P. Zanchetta and S. V. Bozhko, “Accelerated electromechanical modeling of a distributed internal combustion engine generator unit”, *Energies*, 2012, 5, 2232-2247.

[15] S. Das and B. Subudhi, “A H_∞ robust active and reactive power control scheme for a PMSG-based wind energy conversion system”, *IEEE Trans. Energy Conver.*, Vol. 33, N0. 3, pp. 980-990, Sept. 2018.

[16] J. Kim, S. H. Lee, and J. W. Park, “Inertia-free stand-alone microgrid—Part II: Inertia control for stabilizing DC-link capacitor voltage of PMSG wind turbine system”, *IEEE Trans. Ind. Appl.*, Vol. 54, No. 5, pp. 4060-4068, Sept./Oct. 2018.

[17] M. J. Dehkordi, S. V. Zadeh and J. Mohammadi, “Development of a combined control system to improve the performance of a PMSG-based wind energy conversion system under normal and grid fault conditions”, *IEEE Trans. Energy Conver.*,Vol. 34, No. 3, pp.1287-1294, Sept. 2019.

[18] A. D. Hansen, F. Iov, P. Sorensen, N. Cutululis, C. Jauch and F. Blaabjerg, “ Dynamic wind turbine models in power system simulation Tool DigSILENT”, *Riso National Laboratory*, Technical University of Denmark, August, 2007.

Chapter 4
Evaluation of Different PMSG Side Converter Control Schemes

4.1 Introduction

In this chapter, different control strategies for the generator side converter are discussed and applied to the proposed gas engine generator system with a permanent magnet synchronous generator (PMSG). These control schemes can be mainly divided into three types namely; (1) zero d-axis current (ZDC) control, (2) unity power factor (UPF) control and (3) constant stator voltage (CSV) control. The CSV control method was explained in Chapter 3. Therefore, only the ZDC control and the UPF control methods are presented in the following subsections.

These control methods have their own advantages and disadvantages with respect to performance indices and characteristics such as torque versus speed, torque versus current, and power factor. As can be seen from the name of ZDC control, it can be achieved by considering the d-axis stator current as zero. The ZDC control provides a linear relationship between the stator currents and electromagnetic torque. This control can be easily implemented for generator-side converter [1, 2]]. ZDC control is almost independent from the speed range of the generator. Therefore this control structure can be used for many types of PMSGs. Like CSV, the voltage regulation of DC link voltage can be performed in a proper way in ZDC control. Easy implementation is a merit of ZDC control; however, its own demerit is the low power factor.

The UPF control keeps a constant phase angle between the stator voltage and current vectors in all operating conditions [3, 4]. The UPF control optimizes the system's apparent power (volt–ampere requirement) by maintaining the power factor at unity; however, its main drawback is yielding a very low torque per unit current ratio. In order to analyze the transient performance of the PMSG system with different control methods in the generation side converter, several simulations are performed under step load change conditions in the PSCAD/EMTDC software environment.

4.2 Zero d-axis current control

This control scheme is performed in the rotor reference frame in which the voltage vector is aligned on the q-axis component and the d-axis is aligned to the stator flux vector. The magnitude of stator current i_s can be calculated from the d-axis current component i_{ds} and the q-axis current component i_{qs} as written in (4.1).

$$i_s = \sqrt{i_{ds}^2 + i_{qs}^2} \tag{4.1}$$

From (4.1), when the d-axis current component i_{ds} is controlled to be zero, the stator current i_s is equal to the q-axis current component i_{qs}. Thus, the active and reactive powers of PMSG become

$$P_s = v_{qs} i_{qs} \tag{4.2}$$

$$Q_s = -v_{ds} i_{qs} \tag{4.3}$$

Hence, the dc side voltage v_{dc} can be controlled through i_{qs} . Then, the control structure of the proposed stand-alone gas engine generation system with the ZDC control for the PMSG side converter is shown in Fig. 4.1. It consists of three PI controllers, decoupling factors and feed-forward terms. Thus, PI 1 in Fig. 4.1 is a dc-link voltage controller which corresponds to active power. PI 4 and PI 3 are corresponding to the d- and q-axis current controllers, respectively. The outputs of current controllers e_d^*, e_q^* are the voltage reference signals of SVPWM for generating gate signals to the PMSG side converter.

In this control scheme, the decoupling terms are $\omega_e L i_{ds}$, $\omega_e L i_{qs}$, and the feed forward term is $\omega_e \psi_m$. As the control scheme is implemented in the rotor reference frame, an encoder is necessary to measure the rotor position θ_r for each transformation of three-phase system to two-phase system. With this control scheme, the generator provides the maximum possible torque at the minimum current and can minimize the resistive losses in the generator. However, the converter rating increases in this control method as the reactive power of the generator is not zero.

The major disadvantage of ZDC control is un-suitable for salient-pole synchronous generators as optimal operation cannot be achieved with i_{ds}=0 [5, 6].

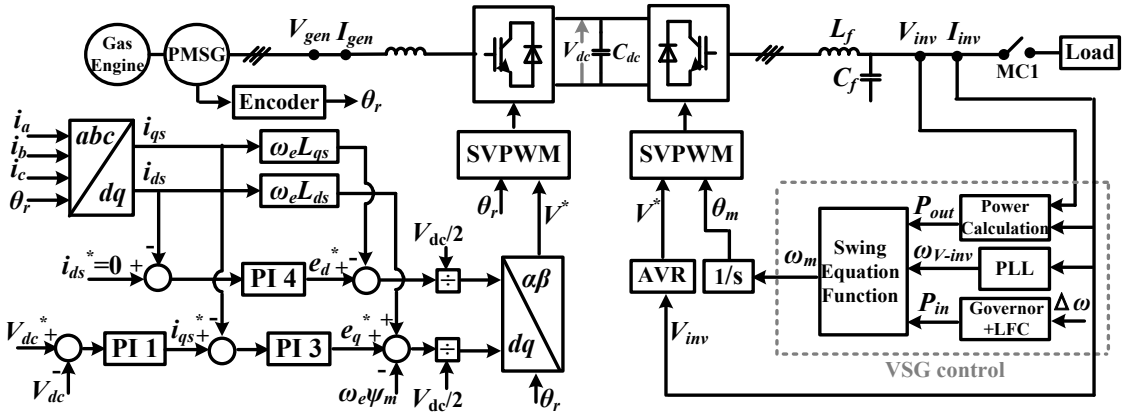

Figure 4.1 Control structure with the ZDC control in the PMSG side converter

4.3 Unity power factor (UPF) control

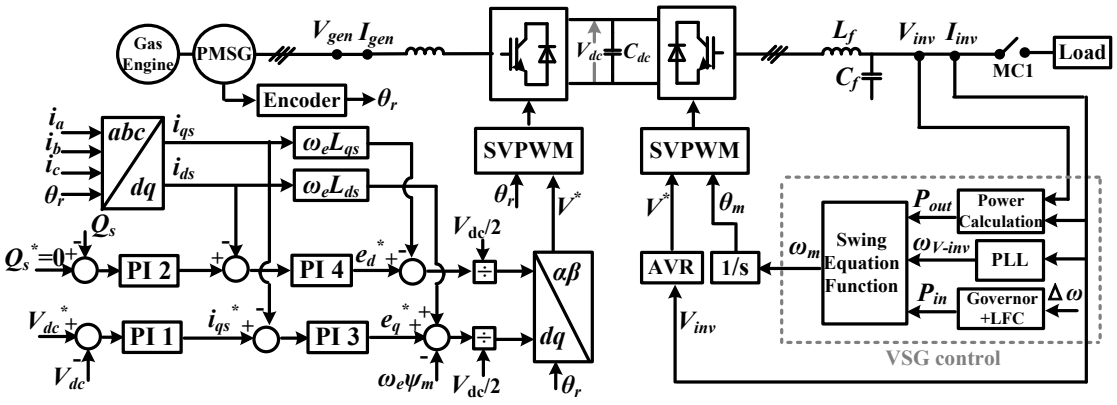

Figure 4.2 Control structure with the UPF control in the PMSG side converter

The d-axis current component i_{ds} can also be used to achieve the unity power factor operation of the PMSG as shown in Fig. 4.2. In this figure, the reactive power reference is set as zero to operate the PMSG with unity power factor. Thus, the reactive power controller PI 2 is included and its output is used as the reference current for i_{ds} control loop. The other controllers perform the same functions as explained in the ZDC control method. Same as in the ZDC control, an encoder is necessary to measure the rotor position θ_r for each transformation of three-phase system to two-phase system. As the reactive power of generator is controlled to be zero, the converter rating can be minimized by this control method.

In the UPF control strategy, the stator current is controlled to fully compensate reactive power at the generator stator [7]. However, as the stator voltage is not directly controlled, over/under voltage issues may arise.

4.4 Simulation results

In order to study the transient performance of the proposed gas engine generator system with different control methods for the PMSG side converter, several simulations are performed under step load change conditions in the PSCAD/EMTDC software environment. . The simulation parameters of the PMSG, the VSG control and the circuit parameters are the same as listed in Tables 3.1, 3.2 and 3.3 of Chapter 3. The proportional gain and the time constant of the reactive power controller PI 2 in the UPF control are set as K_p = 10 and T_i = 0.1 s. The simulation condition is also the same as presented in Section 3.3 of Chapter 3.

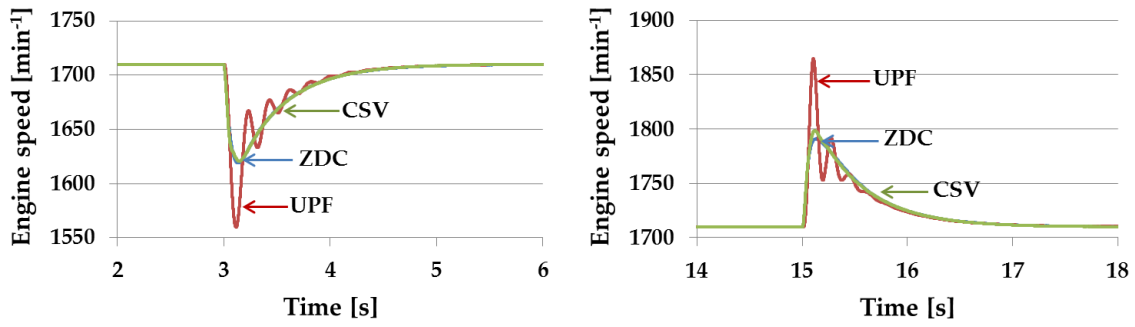

(a) (b)

Figure 4.3 The engine speed (a) loading case, (b) load removal case

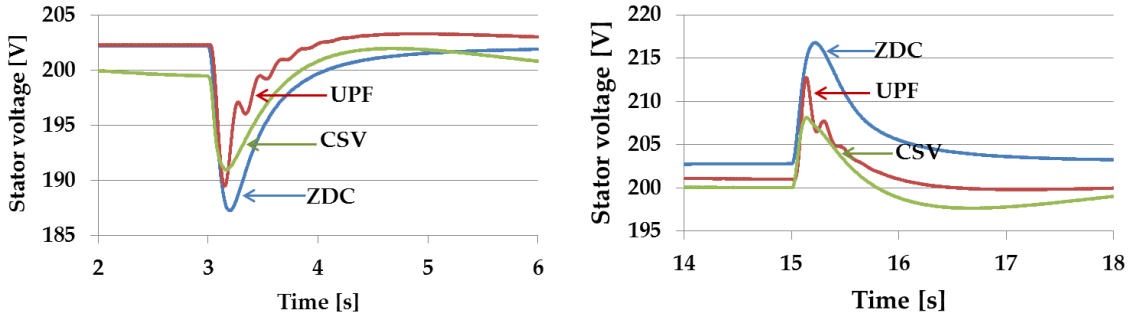

(a) (b)

Figure 4.4 The stator voltage (a) loading case, (b) load removal case

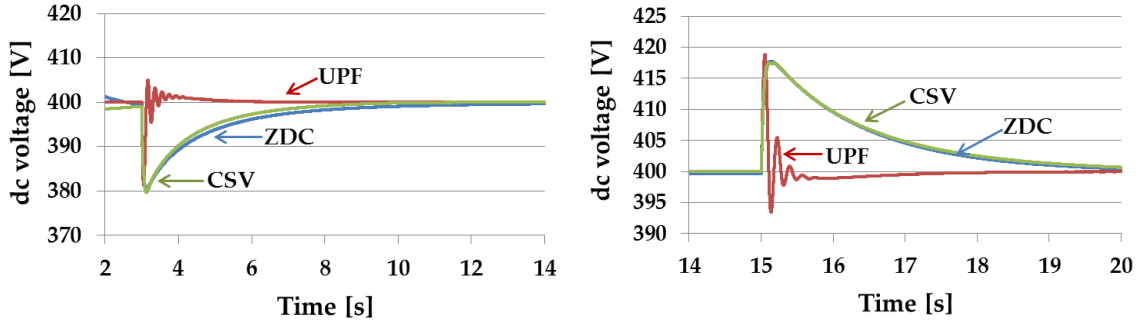

(a) (b)

Figure 4.5 The dc-link voltage (a) loading case, (b) load removal case

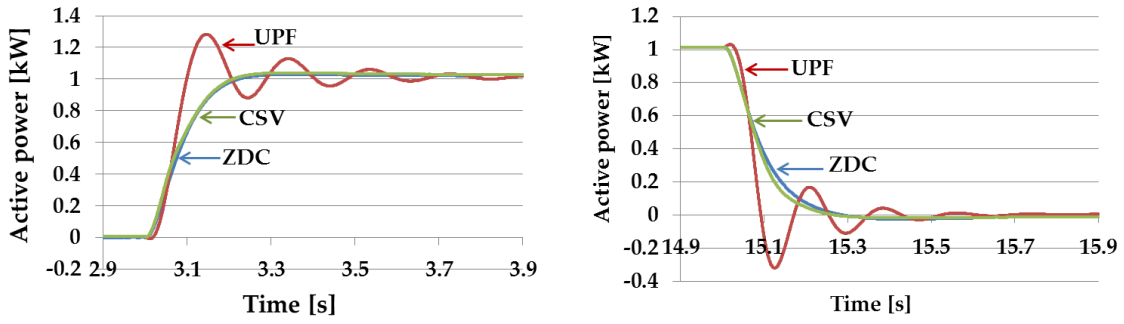

(a) (b)

Figure 4.6 The generator output active power (a) loading case, (b) load removal case

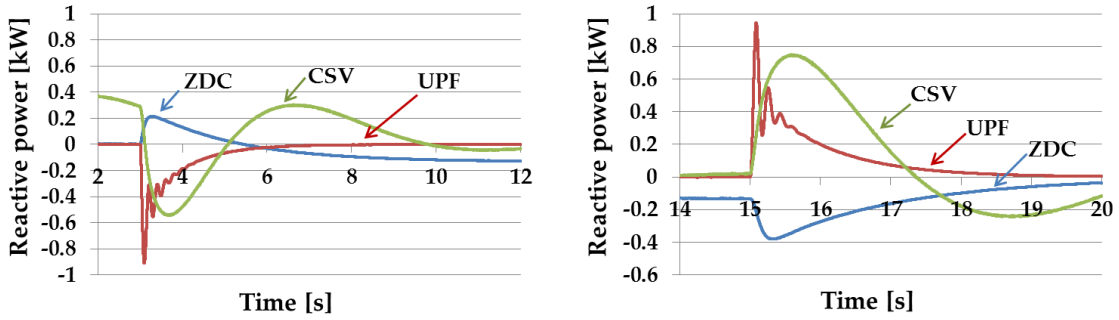

(a) (b)

Figure 4.7 The generator output reactive power (a) loading case, (b) load removal case

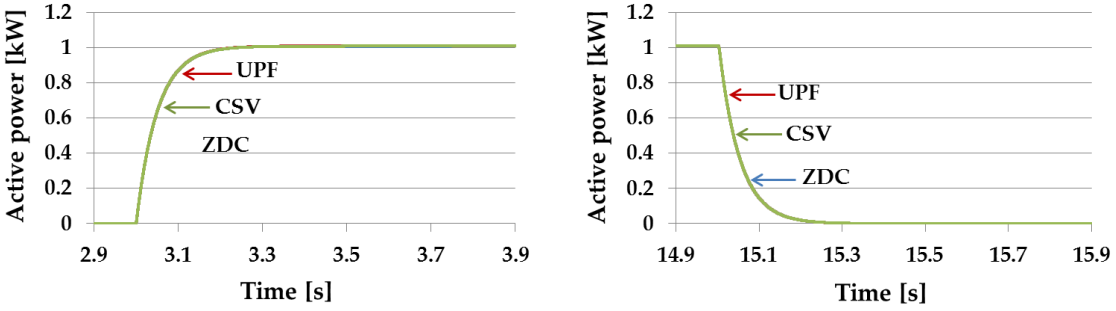

(a) (b)

Figure 4.8 The inverter output active power (a) loading case, (b) load removal case

The simulation results of the engine speed during the step load changes are shown in Fig. 4.3. For both loading and unloading cases, the engine speed in the case of UPF control method is more oscillatory. The engine speed transients of the CSV control and

the ZDC control methods are almost similar. The stator voltage responses are illustrated in Fig. 4.4, which shows that the stator voltage is deviated from its rated value with the ZDC and UPF control methods. By the CSV control, the stator voltage is controlled to follow its reference value after the transient. Moreover, the amount of voltage variations is the lowest during the transient. The dc-link voltage responses to the load changes are shown in Fig. 4.5. The dc-link voltage responses of the ZDC method and the CSV method are almost the same. With the UPF control, there are some oscillations in the dc-link voltage waveform.

The waveforms of generator output active power are shown in Fig. 4.6. The ZDC method and the CSV method output similar active power responses with smooth transitions. The UPF control method makes some oscillations during the transient period. The generator output reactive power responses are presented in Fig. 4.7. With the ZDC control, there can be seen the negative reactive power in the steady state condition. With the CSV control, the reactive power has a large oscillation during the load transition and then it recovers to zero value in the steady state condition. With the UPF control, the reactive power is well controlled at zero value in the steady state condition. The inverter output waveforms are shown in Fig. 4.8. The load power transitions have a smooth change in all cases.

Some investigations show that the operating range of a PSMG with the UPF control in comparison of other two control methods is limited [5]. This is due to the UPF constraints specified by stator inductances, limiting the stator current magnitude and angle [11]. This limitation is specifically obvious in the speed range and limits the turbine's mechanical power available at rated and high speeds. That is why the PMSG with the CSV and the ZDC performs better, especially at rated speed.

From the simulation results, it can be said that each control method can be well applied to the proposed gas engine system for approaching the targeted control objectives. However, as can be seen from the waveforms, a better system performance is obtained with the CSV control method. Moreover, an encoder is not used in this control method and therefore the CSV control method is simpler than the other two methods.

4.5 Summary

This chapter addressed the application of three different control strategies for the generator side converter in a PMSG. These control strategies are CSV control, ZDC control, and UPF control. The CSV control is discussed in Chapter 3 in detail, and the control schemes of the ZDC control and UPF control methods are presented in this chapter.

In order to investigate the transient performance of the gas engine generator system in the presence of different control methods for the PMSG side converter, some nonlinear simulations are carried out in the PSCAD/EMTDC software environment. The performance of the mentioned three control methods are examined under step load change conditions, and the results are compared.

It is shown that each control method has its own advantages and disadvantages with respect to wide range of performance indices and characteristics such as speed, dc-link voltage, active power and reactive power responses. However in general, the performed simulations confirmed that a better system performance can be achieved by using the CSV control method. Moreover, due to its encoder-free feature, the CSV control method is simpler than the other two methods.

References

[1] Chen Z, Hu Y, and Blaabjerg F, "Stability improvement of induction generator-based wind turbine systems," *IET Renewable Power Generation* 2007, pp.81–93.

[2] Mendis N, Muttaqi KM, Sayeef Saad, Perera S, "Standalone operation of wind turbine-based variable speed generators with maximum power extraction capability", *IEEE Trans. on Energy Conversion,* vol. 27, no.4, pp. 822-834, 2012.

[3] Liu Z, Liu C, Li G, Liu Y, Liu Y, "Impact study of PMSG-based wind power penetration on power system transient stability using EEAC theory", *Energies* 2015; 8: 13419-13441.

[4] A. I. Maswood and L. Fangrui, "A unity-power-factor converter using the synchronous-reference-frame-based hysteresis current control, *IEEE Trans. Ind. Appl.*, vol. 43, no. 2, pp. 593–599, Mar./Apr. 2007.

[5] B. Wu, Y. Lang, N. Zargari, S. Kouroi, "Power Conversion and control of Wind Energy Systems", Wiley, 2011. https://doi.org/10.1002/9781118029008.

[6] Huang K H K, S. H. S. Huang, F. S. F. She, B. L. B. Luo, and L. C. L. Cai, "A control strategy for direct-drive permanent-magnet wind-power generator using back-to-back PWM convert-er", in *Proc. International Conference on Electrical Machines and Systems*, pp.2283–2288.

[7] S. Li, T. A. Haskew, and L. Xu, "Conventional and novel control designs for direct driven PMSG wind turbines," *Electric Power Systems Research*, vol. 80, pp. 328-338, 3// 2010.

[8] Y. Wang, J. Meng, X. Zhang, and L. Xu, "Control of PMSG-based wind turbines for system inertial response and power oscillation damping", *IEEE Trans. Sustainable Energy*, vol. 6, no. 2, pp.565-574, Apr. 2015.

[9] S. Li, M. Cao, J. Li, J. Cao and Z. Lin, "Sensorless-based active disturbance rejection control for a wind energy conversion system with permanent magnet synchronous generator", *IEEE Access*, Digital Object Identifier 10.1109/ACCESS.2019.2938199.

[10] N. D. Dao, D. C. Lee and Sangmin, "A simple and robust sensorless control based on stator current vector for PMSG wind power systems", *IEEE Access*, Digital Object Identifier 10.1109/ACCESS.2018.2889083.

[11] S. H. Qazi and M. W. B. Mustafa, "Technical Issues on Integration of Wind Farms with Power Grid-A Review", *International Journal of Renewable and Sustainable Energy*, 2014, 3, 87-91.

Chapter 5
Conclusion

In response to the challenge of economical harvesting of electrical energy and considering the environmental issues according to the Paris agreement for CO_2 reduction [1], a key solution could be to integrate more and more distributed generators (DGs) in the electric network. In this direction, in most countries like Japan, the capacity of installed inverter-based DGs in power grids is rapidly growing; and a high penetration level is targeted for the next two decades.

However, recent studies have investigated that using the DGs with poor control performance will have some negative impacts on the system dynamics, frequency, voltage, output active/reactive power, harmonic distortion, and other control and operation issues [2]. In consequence, this challenge may significantly limit the quality of system operation, as well as the overall system performance and stability.

In response to above mentioned challenge, the present thesis is mainly focused on proposing new control solutions based on the virtual synchronous generator (VSG) concept and controlled active power rectifier. The developed approaches were supplemented by some computer-based simulations and one laboratory-based experiment. The main objective was to improve the PMSG-based stand-alone gas generator system stability and performance in the presence of a serious load changes. The main body of research has been organized in four past chapters, and here, I briefly summarize the research steps, concluding remarks, and achievements. The future steps of this works have also been emphasized.

5.1 Research summary and achievements

In this dissertation, the role of gas engine in DG system was briefly presented. The weak point of gas engine generator under transient conditions was stated. The transient performance of a stand-alone gas engine generator was demonstrated. The VSG control concept which was a recent popular control method for the grid-connected inverter control was proposed for the control of load side inverter in a stand-alone gas engine generation system. The VSG control structure was presented. The advantage of virtual inertia provided by the VSG-controlled inverter was evaluated in a comparison of the same system configuration with a conventional CVCF-controlled inverter. Using the proposed VSG-controlled inverter, two rectifier topologies are connected in generator side converter of the gas engine system and the system responses to the sudden load changes were investigated.

First, the gas engine generator with the diode rectifier and the VSG-controlled inverter was studied. In this configuration, an external energy storage system (ESS) was added to the dc-link and the system performance was compared with ESS and without ESS. The ESS energy was controlled in accordance with charging and discharging modes. In this system, the dc-link voltage was not directly controlled in both sides of controllers. Therefore, the dc-link voltage was decreased under loading condition and the overall system efficiency might be affected. However, the system with ESS provided a temporary energy supply during transient periods and the speed variations were reduced. As a result, this system covered the slow response of engine's mechanical dynamics by the electrical side controller. From the system stability and reliability point of view, the ESS should be used. From the economical point of view, the use of ESS was costly and the control structure was complicated.

Secondly, instead of a diode rectifier, an active rectifier is applied to the PMSG side converter in order to obtain a full controllability of the system. Among different control methods of PMSG, the constant stator voltage (CSV) control approach was firstly applied for the PMSG side converter control. Thus, the PMSG side converter was controlled to provide the direct dc-link voltage control and the stator voltage control by controlling the d and q component currents. For the sake of showing the effectiveness of the proposed control scheme, several computer simulations were performed for the step load change test while the generator unit was working in stand-alone operation mode. In comparison with a diode rectifier-based system, the system with active rectifier was significantly effective regarding generator current harmonic reduction. Thus, an improvement in generator efficiency was confirmed.

Finally, three different control strategies for the generator side converter were studied. These control strategies were the CSV control, the zero d-axis current (ZDC) control, and the unity power factor (UPF) control. In order to investigate the transient performance of the gas engine generator system in the presence of different control methods for the PMSG side converter, some nonlinear simulations were carried out in the PSCAD/EMTDC software environment. The performance of mentioned three control methods were examined under step load change conditions, and the results were compared.

It is shown that each control method had its own advantages and disadvantages with respect to wide range of performance indices and characteristics such as speed, dc voltage, active power and reactive power responses. However in general, the performed simulations confirmed that a better system performance can be achieved by using the CSV control method. Moreover, due to the encoder-less feature, the CSV control method is simpler to be applied than the other two methods.

5.2 Further research steps

The present research in this thesis can be considered as an initial step to study the PMSG-based stand-alone gas generator system control by application of a combination of active rectifier and VSG control. More efforts are needed to further enhance the stability and performance of the stand-alone operation of a gas engine generator.

Some future steps can be considered as:

- Conducting more experimental tests for evaluating and validation of the proposed control strategy for the application of active rectifier and VSG control.
- Improving the VSG control scheme to produce inertia and damping parameters, adaptively.
- Examining other advanced control methodologies such as robust and intelligent adaptive control techniques to further improve system dynamic performance for all three subsystems, i.e, generation side rectifier, dc-link voltage control, and load side inverter.
- Using model-free based control synthesis methods known as data-driven control techniques for control of a PMSG-based stand-alone gas generator system.

References

[1] Available online: https://ec.europa.eu/clima/policies/international/negotiations/paris_en.

[2] H. Bevrani, B. François, and T. Ise, *Microgrid dynamics and control*. John Wiley & Sons, 2017.

Acknowledgments

First and foremost, I would like to express a deep sense of gratitude to my supervisor, Professor Toshifumi Ise for his immerse knowledge and for his guidance throughout my research. His valuable guidance, kind patience and constant encouragement enabled me to complete this dissertation.

I would also like to express my heartfelt thanks to Professor Yushi Miura for his persistent help and valuable advices on my researches. I would also like to express my sincere gratitude to Assistant Professor Jia Liu for his kind assistance given in many ways. This dissertation would not have been possible without the continuous support and guidance from my supervisors.

My special thanks also go to Professor Shigemasa Takai for his careful review on this dissertation and insightful comments. Besides, my sincere thanks to the other members of my dissertation committee: Professor Tsuyoshi Funaki, Professor Tomoo Ushio, Professor Hiroyuki Shiraga and invited Professor Shigekazu Sakabe for their valuable comments and suggestions for improving the quality of my dissertation.

I am deeply indebted to Professor Hassan Bevrani in the Department of Electrical and Computer Engineering, University of Kurdistan, Iran, for his precious advices, support and encouragement during the co-authoring of my journal papers.

My grateful acknowledgements also go to Yanmar Co., Ltd. for providing the financial assistance, necessary materials and helpful advices during the co-operative research work. I also wish to acknowledge Mr. Kagawa, Mr. Banjo and Mr. Takeyama of Ise Laboratory for their kind help and for sharing their knowledge during the experimental work of this research.

I would like to present my most sincere gratitude to the Japanese Ministry of Education, Culture, Sports, Science and Technology, for giving me a great opportunity to study in Japan and for granting me the MEXT scholarship.

I would like to extend my gratitude to the Ministry of Education, Myanmar, for giving me a chance to continue my studies until this dissertation is finished.

Finally, my endless thanks go to my parents and my only elder brother who always support me, believe in me and encourage me to follow my dreams in different circumstances.

List of Publications

Journal Publications (with review)

[1] Htar Su Hlaing, Jia Liu, Yushi Miura, Hassan Bevrani and Toshifumi Ise, "Enhanced Performance of a Stand-alone Gas-Engine Generator Using Virtual Synchronous Generator and Energy Storage System," *IEEE Access*, Vol.7, 2019, DOI (identifier) 10.1109/ACCESS.2019.2957890, pp. 176960- 176970

[2] Htar Su Hlaing, Jia Liu, Hassan Bevrani and Toshifumi Ise, "PMSG Control for a Stand-alone Gas Engine Generator Using Active Rectifier and VSG-controlled Inverter," *Energies* 2020, *13*, 233, doi:10.3390/en13010233

Papers Presented at International Conference
(Oral presentation, with review)

[1] Htar Su Hlaing, Yushi Miura, Toshifumi Ise, "A Permanent Magnet Synchronous Generator Control Approach for Stand-alone Gas Engine Generation System", IEEE 8th International Power Electronics and Motion Control Conference (IPEMC-ECCE Asia), May 2016,Hefei, P.R. China

Papers Presented at Domestic Conferences
(Oral presentation, without review)

[1] Htar Su Hlaing, Yushi Miura and Toshifumi Ise: "Application of Back-to-Back Converter to an Engine Generation System using a Permanent Magnet Synchronous Generator", Technical Meeting on Power Engineering and Power System Engineering, Touhoku University, Japan, September 16-18, PE-15-069, PSE-15-091, pp. 11-16 (2015)